



# Legionella pneumophila PPlase Mip Interacts with the Bacterial Proteins SspB, Lpc2061, and FlaA and Promotes Flagellation

Mustafa Safa Karagöz,<sup>a</sup> Can Murat Ünal,<sup>a</sup> Benjamin E. Mayer,<sup>b</sup> Mathias Müsken,<sup>c</sup> José Manuel Borrero-de Acuña,<sup>d</sup> Michael Steinert<sup>a,c</sup>

<sup>a</sup>Institut für Mikrobiologie, Technische Universität Braunschweig, Braunschweig, Germany

<sup>b</sup>Computational Biology and Simulation, Technische Universität Darmstadt, Darmstadt, Germany

<sup>c</sup>Helmholtz Centre for Infection Research, Braunschweig, Germany

<sup>d</sup>Departamento de Microbiología, Facultad de Biología, Universidad de Seville, Seville, Spain

**ABSTRACT** The peptidyl-prolyl-*cis/trans*-isomerase (PPlase) macrophage infectivity potentiator (Mip) contributes to the pathogenicity and fitness of *L. pneumophila*, the causative agent of Legionnaires' disease. Here, we identified the stringent starvation protein SspB, hypothetical protein Lpc2061, and flagellin FlaA as bacterial interaction partners of Mip. The macrolide FK506, which inhibits the PPlase activity of Mip, interfered with the binding of Lpc2061. Moreover, we demonstrated that the N-terminal dimerization region and amino acid Y185 in the C-terminal PPlase domain of Mip are required for the binding of Lpc2061 and FlaA. The modeling of the interaction partners and global docking with Mip suggested nonoverlapping binding interfaces, and a molecular dynamic simulation predicted an increased stability for the tripartite interaction of Lpc2061, Mip, and FlaA. On the functional level, we demonstrated that Mip promotes *L. pneumophila* flagellation, which is positively influenced by the binding of Lpc2061 and reduced by FK506. Also, *L. pneumophila* mutants expressing the Y185A or the monomeric Mip variant, which bind less Lpc2061, were nonmotile, were less flagellated, and yielded less FlaA when quantified. To our knowledge, this is the first report in which a PPlase and its bacterial interaction partners were demonstrated to influence flagellation.

**KEYWORDS** *Legionella pneumophila*, macrophage infectivity potentiator (Mip), peptidyl-prolyl *cis/trans* isomerase (PPlase), flagella, interactomics

*L. pneumophila*, the causative agent of Legionnaires' disease, naturally inhabits freshwaters and accumulates in biofilms, where it parasitizes intracellularly within different protozoa species (1–3). *L. pneumophila* also thrives in human-made water systems, including air conditioning units and cooling towers (4–7). Infection of humans occurs via the inhalation of *L. pneumophila*-contaminated aerosols, which can lead to severe and life-threatening pneumonia. Upon inhalation, the bacteria mainly invade alveolar macrophages, replicate within a specialized cellular compartment, termed the *Legionella*-containing vacuole (LCV), and cause severe lung damage (8–11).

*L. pneumophila* expresses the macrophage infectivity potentiator (Mip) protein, which was the first genetically identified virulence factor of *L. pneumophila* (12, 13). Deletion of *mip* results in reduced intracellular replication rates in human alveolar macrophages and protozoa during the onset of infection (12, 14, 15). Mip is a basic 24 kDa surface protein (pI 9.8) and possesses an N-terminal signal sequence that is cleaved off while the protein is transported through the cytoplasmic membrane (16). The protein forms a stable homodimer, and the 2.4 Å crystal structure revealed that each monomer consists of an N-terminal dimerization module, a long connecting  $\alpha$ -helix ( $\alpha$ 3), and a C-terminal peptidyl-prolyl-*cis/trans*-isomerase (PPlase) domain (17–20). The fold of the C-terminal

**Editor** Craig R. Roy, Yale University School of Medicine

**Copyright** © 2022 Karagöz et al. This is an open-access article distributed under the terms of the [Creative Commons Attribution 4.0 International license](https://creativecommons.org/licenses/by/4.0/).

Address correspondence to Michael Steinert, [m.steinert@tu-bs.de](mailto:m.steinert@tu-bs.de).

The authors declare no conflict of interest.

**Received** 7 July 2022

**Returned for modification** 10 August 2022

**Accepted** 27 September 2022

**Published** 31 October 2022

domain (residues 100 to 213) is closely related to the human FK506-binding protein 12 (FKBP12) (21, 22). As characteristic of this protein family, the PPlase activity of Mip is inhibited by the macrolides FK506 and rapamycin (23). In a previous nuclear magnetic resonance (NMR) investigation, we were able to solve the solution structure of free Mip<sup>77-213</sup> and the Mip<sup>77-213</sup>/rapamycin complex, confirming their stable interaction (24). Mediated by a hinge in the long  $\alpha$ -helix, both FKBP domains of the dimerized Mip are subject to large fluctuating movements, which allows for the flexible cooperative binding of potential target structures (25).

Previous studies employing genetic and biochemical methods together with different infection models revealed that Mip impacts the course and outcome of infection on multiple levels (16, 19, 26, 27). Since the PPlase domains of all PPlases contain highly conserved amino acids within their FK506-binding pockets, we generated single substitution mutants, in which Asp142 was replaced by leucine and Tyr185 was replaced by alanine. The purified recombinant proteins exhibited a pronounced loss of PPlase activity in *in vitro* PPlase assays (6.2% for the D142L mutant and 2.0% for the Y185A mutant). When the same site-specifically mutated variants of *mip* were used to complement the *L. pneumophila*  $\Delta$ *mip* mutants in infection studies, wild-type phenotypes with *Acanthamoeba castellanii* or human macrophage-like cell lines were observed (16). We concluded that either additional properties other than the PPlase activity are important during intracellular infection or the residual enzymatic activity of the mutated Mip was still sufficient for the PPlase-dependent phenotypes. In contrast, *L. pneumophila* strains that were unable to dimerize or had a low PPlase activity were significantly attenuated in a guinea pig infection model (19). This was further confirmed when Mip-deficient bacteria were found to be attenuated and unable to disseminate systemically in guinea pigs (26).

The different effects of a reduction in PPlase activity in cell culture systems and guinea pig infections suggested additional functions of Mip during the more complex infection of guinea pigs. In accordance, the apicobasal transmigration of *L. pneumophila*  $\Delta$ *mip* mutants were strongly impaired in *in vitro* assays that modeled the lung epithelial barrier, including the extracellular matrix (ECM). Further systematic biochemical binding studies revealed that Mip binds to collagen IV in the ECM. This suggests that there is a concerted action of Mip and proteolytic enzymes that leads to ECM-degradation and transmigration (26). The Mip-collagen IV interaction was further elucidated by utilizing peptide arrays and coprecipitation studies, and a distinct 13 amino acid-long sequence (IPPCPSGWSSLWI; P290) was identified within the globular non-collagenous (NC1) region of collagen IV as the target of Mip. Synthetic P290 interfered with Mip-binding to collagen IV in a dose-dependent manner and accordingly reduced *in vitro* bacterial transmigration. NMR studies of the P290-Mip complex revealed that with its central residues, P290, like rapamycin, occupies the catalytic cleft, thereby forming a hairpin. Its terminal residues make contact with the amino acids of Mip that are outside the catalytic groove, which further stabilizes the complex (28).

Although being the first identified virulence factor of *L. pneumophila* and the first virulence-associated PPlase, it is still not known how Mip exerts its diverse functions. In this study, we use an interactomic approach and show that stringent starvation protein B (SspB, LPC\_0434), hypothetical protein Lpc2061 (LPC\_2061), and flagellin (FlaA, LPC\_0756) are *in vivo* bacterial interaction partners of Mip. After the validation of these *L. pneumophila* proteins, we demonstrate that FK506 inhibits the Mip-Lpc2061 interaction. We also report that the dimerization region and the amino acid Y185 of Mip are crucial for the binding of Lpc2061, which is strengthened by FlaA. Via the modeling of the respective interaction partners with AlphaFold v2.0 and the global *in silico* docking of each partner with Mip, we further portray the putative binding interfaces. We demonstrate that Mip-deficient bacterial cells yield less FlaA protein and result in reduced flagellum formation. This is, to our knowledge, the first report showing the promoting effect of a PPlase on bacterial flagellation.

**TABLE 1** Strains and primers used in this study

Strain	Specification	Reference
<i>Legionella pneumophila</i> Corby wt	Media without antibiotics	74
<i>Legionella pneumophila</i> Corby $\Delta$ mip	Kanamycin resistant	16
<i>Legionella pneumophila</i> Corby $\Delta$ flaA	Kanamycin resistant	55
<i>L. pneumophila</i> Philadelphia 1 JR32-2.3 (Mip D142L)	Kanamycin, chloramphenicol, and streptomycin resistant	16
<i>L. pneumophila</i> Philadelphia 1 JR32-2.2 (Mip Y185A)	Kanamycin, chloramphenicol, and streptomycin resistant	16
<i>L. pneumophila</i> Philadelphia 1 JR32-2.4 (Mip monomer)	Kanamycin, chloramphenicol, and streptomycin resistant	19
<i>E. coli</i> DH10 $\beta$		
<i>E. coli</i> BL21		
pet52b with LpSspB in <i>E. coli</i> BL21	Ampicilin resistant for the expression of LpSspB with StrepTag	This study
pet22b with Lpc_2061 in <i>E. coli</i> BL21	Ampicilin resistant for the expression Lpc2061 with HisTag	This study
Primers		
AGCGTCGACATGGCAATGACATCAAACAAACC	sspb_fw_Sall	
AGCGAGCTCCTACTTTACCAGTTTTAGTGATGG	sspb_rev_Sacl	
AGCGAGCTCAGCCCTGTAGGCTCTGATTGTA	2061_nosig_Sacl_fv	
AGCGTCGACTTAACCTTTTAGACCAACTGGGAAAA	2061_rv_Sall	

## RESULTS

**Immunoprecipitation reveals stringent starvation protein SspB, hypothetical protein Lpc2061, and flagellin (FlaA) as *in vivo* interaction partners of Mip.** To identify *in vivo* interaction partners of Mip, a mixture of two monoclonal Mip-antibodies, 2D8 and 22/1, was used for coimmunoprecipitation. While antibody 2D8 binds specifically to a C-terminal epitope, antibody 22/1 recognizes an epitope at the N terminus of Mip (unpublished data). Bacterial cell membranes of the wild-type strain *L. pneumophila* Corby and the corresponding isogenic  $\Delta$ mip mutant strain were solubilized and coimmunoprecipitated (Table 1). Eluted proteins were resolved by SDS-PAGE and stained with silver or Coomassie blue (Fig. 1A–F). As controls, antibodies without any cell material and recombinant Mip were visualized on the gel. Bands at 50 and 25 kDa originated from the light and heavy chains of the antibodies, respectively, and were excluded from the further assessment of interaction partners. Protein eluates derived from membrane fractions of the *L. pneumophila* wild-type strain showed a clear band at a relative molecular weight of 28 kDa (Fig. 1A), where the recombinantly produced Mip (25 kDa) was detected as well, though this was absent in the  $\Delta$ mip strain (Fig. S1). Additionally, we expanded the identification of the Mip-specific interactome by implementing *in vivo* formaldehyde (FA)-driven cross-linking. This cross-linking should identify interaction partners which bind to a lower extent, with weaker strength, where the interaction is transient, or where partners are simply pulled away by stringent washing conditions. Thus, cultures were alternatively treated with different concentrations of FA as a cross-linking agent prior to cell harvesting and fractionation, followed by the detergent-solubilization of the membrane fractions. Cross-linking with different FA concentrations gave rise to additional protein bands, suggesting further interaction partners. Cross-linking with 0.5% (vol/vol) FA revealed the largest number of protein bands (Fig. 1B), many of which vanished progressively with higher concentrations (Fig. S2). Accordingly, immunodetection assays employing wild-type-derived membrane fractions revealed the major chromogenic signal at a relative molecular weight of 28 kDa, which corresponds to Mip and indicates proper purification (Fig. 1B). Additionally, the *L. pneumophila*  $\Delta$ mip mutant produced neither Mip nor additional bands when superimposed upon the stand-alone antibody fraction, as visualized by silver-staining. This suggests that no unspecific binding of proteins to the column material occurred (Fig. S1 and S2). Coomassie stained SDS gels and Western blots (WB) after coimmunoprecipitation (CoIP) also revealed a 25 kDa band, which refers to purified recombinant Mip (Fig. 1C–F).

To identify the Mip interaction partners, all of the eluted proteins from wild-type bacteria, including those with and without FA supplementation, were subjected to LC/MS (Table 2). SspB (LPC\_0434), a 14.6 kDa protein according to MS, coeluted with Mip

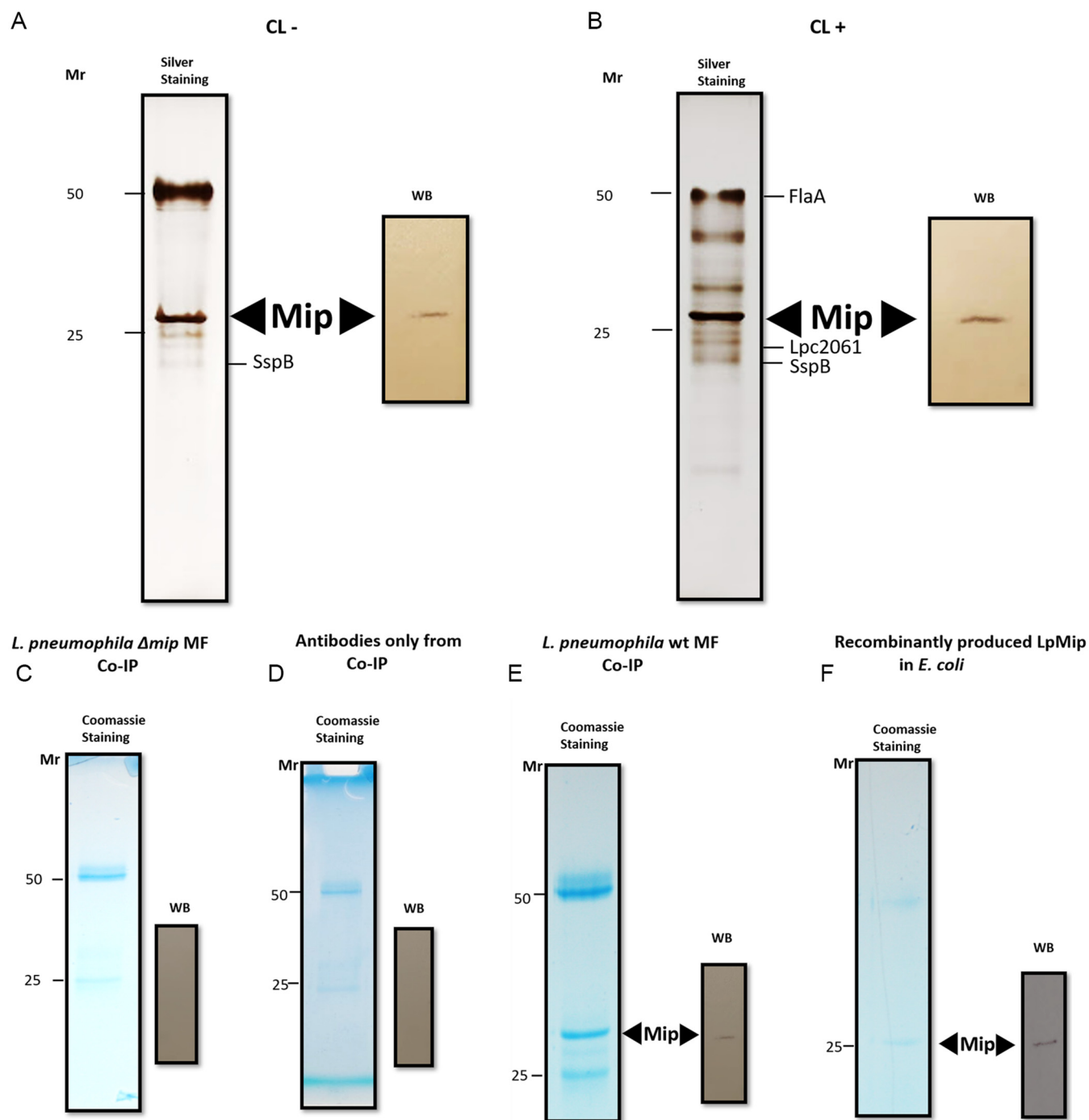


**FIG 1** Identification of bacterial interaction partners of *L. pneumophila* Mip by coimmunoprecipitation. Bacterial cell membrane fractions (MF) were solubilized and coimmunoprecipitated with a mixture of monoclonal Mip-antibodies 2D8 and 22/1. Eluted proteins were resolved by SDS-PAGE and silver stained. (A) Mip eluates from not cross-linked (CL<sup>-</sup>) homogenates of *L. pneumophila* cells that were grown to the prestationary-phase resulted in a band at 28 kDa, which corresponds to Mip (left). The identity of Mip was confirmed via the Western blotting (WB) of the same fraction with anti-Mip antibodies (right). (B) To identify additional weaker interaction partners of Mip *in vivo*, cross-linking (CL<sup>+</sup>) with 0.5% (vol/vol) formaldehyde was performed prior to coimmunoprecipitation, SDS-PAGE, silver staining (left), and Western blotting (right). The CL gave rise to additional protein bands. The purified bands from the wild-type bacteria with and without formaldehyde cross-linking were subsequently subjected to LC/MS analyses for protein identification. Coomassie stained SDS gels and Western blots after coimmunoprecipitation (CoIP) revealed a 25 kDa band, which refers to purified recombinant Mip (C-F). Moreover, the elution fractions showed heavy and light chains of antibodies at 50 and 25 kDa in the Coomassie stains. For the uncropped Western blots, see Fig. S1.

**TABLE 2** Mass spectrometry analysis from Gel, results of purified Mip with coimmunoprecipitation

Protein	NCBI protein ID	Mass in kDa	Gene locus	FA 0%	FA 0,5%	Homology	Description
Mip	<a href="#">ABQ56418</a>	24.849	Lpc_2500 975812-976513	+	+	FK506 Binding Proteins	Macrophage infectivity potentiator
SspB	<a href="#">ABQ54423</a>	14.623	Lpc_0434 3231405-3231800	+	+	Stringent starvation proteins	Stringent starvation protein B ClpXP protease specificity enhancing factor
Lpc2061	<a href="#">ABQ55991</a>	15.773	Lpc_2061 2911556-2911993	–	+	Homologs only in <i>Legionellaceae</i> family	Hypothetical protein Structural homology, AlphaFold 2.0 predicted model, to glycoside hydrolases according ProFunc database
FlaA	<a href="#">ABQ54733</a>	47.858	Lpc_0756 1546346-1547773	–	+	Flagellin known as FliC in other organisms	Flagellin main flagellar monomer

without adding cross-linking agents, as determined by LC-MS/MS analysis. Cross-linking experiments coupled with LC-MS/MS analysis led to the identification of hypothetical protein Lpc2061 at 15.7 kDa and of the main flagellar monomer FlaA (LPC\_0756) at approximately 48 kDa. SspB (LPC\_0434) also coeluted after cross-linking. Interestingly, the silver-stained gels revealed additional protein bands which were not detected in the LC/MS analysis.

A basic BLAST search using the NCBI database resulted with 67 homologous proteins to the hypothetical protein Lpc2061, 63 of which belonged to the *Legionellaceae* family. The other four hits were proposed to be hypothetical proteins from the Gammaproteobacteria *Aquicella lusitana*, *Aquicella siphonis* and *Legionella gormanii*. To gain further knowledge about the identified proteins and their putative functions, the ProFunc database was used. Lpc2061 showed homology to the glycoside hydrolase family. Taken together, the non-linking and cross-linking coimmunoprecipitation experiments with Mip revealed binding proteins of variable interaction strengths, which encompass diverse functional categories.

**Validation of Mip interaction partners and influence of FK506 on coimmunoprecipitation.** To validate the identified interaction partners of Mip by a complementary approach, tagged variants of SspB and Lpc2061 were recombinantly produced in *E. coli*, whereas the native flagellin was purified from wild-type *L. pneumophila* (Table 1). Recombinant Mip was immobilized on magnetic beads coated with Protein G-antibodies as previously specified and then loaded with 1 mg of each purified interaction partner. The degree of association in terms of strength and stability displayed by each of the partners was relatively quantified with respect to band intensity in Coomassie-stained and Western blotted gels by using the ImageJ band intensity determination tools (Fig. 2A–F). When SspB was pulled down with immobilized Mip, a band at 15 kDa, along with Mip, appeared on the gel, which was further confirmed by Western blotting (Fig. 2A). The intensity of the SspB band on the PVDF membrane was the highest, with a relative value of 5028.832 intensity units (Table 3). Purified Lpc2061 coeluted with Mip resulted in a clear band at 15 kDa, which showed a positive signal for the 6×His-Tag in Western blotting (Fig. 2B). The band of Lpc2061 emitted a relative value of 4687.276 intensity units (Table 3). Besides Lpc2061, Mip was successfully copurified as a 25 kDa band, and this was detected in the Western blot. When isolated flagella were added to immobilized Mip, clearly visible bands were detected at about 50 kDa and 25 kDa which correspond to FlaA and Mip, respectively (Fig. 2C). The intensity of the band from the Western blotting was, at 4314.004 units, the lowest compared to the other partners (Table 3). Since the antibodies used for the coimmunoprecipitation showed no signal for the purified interaction partners, the coelution is regarded as specific to the interaction with Mip (Fig. S3 and S4). These data confirm the interactions of Mip with the respective proteins, with SspB being the strongest binder, followed by Lpc2061 and FlaA.

Since Mip is a FK506 binding protein (FKBP), we also assessed whether FK506 is able to prevent the binding of SspB, Lpc2061, and FlaA to recombinant Mip. Hence, we performed the aforementioned coimmunoprecipitation approach by adding 20  $\mu$ M

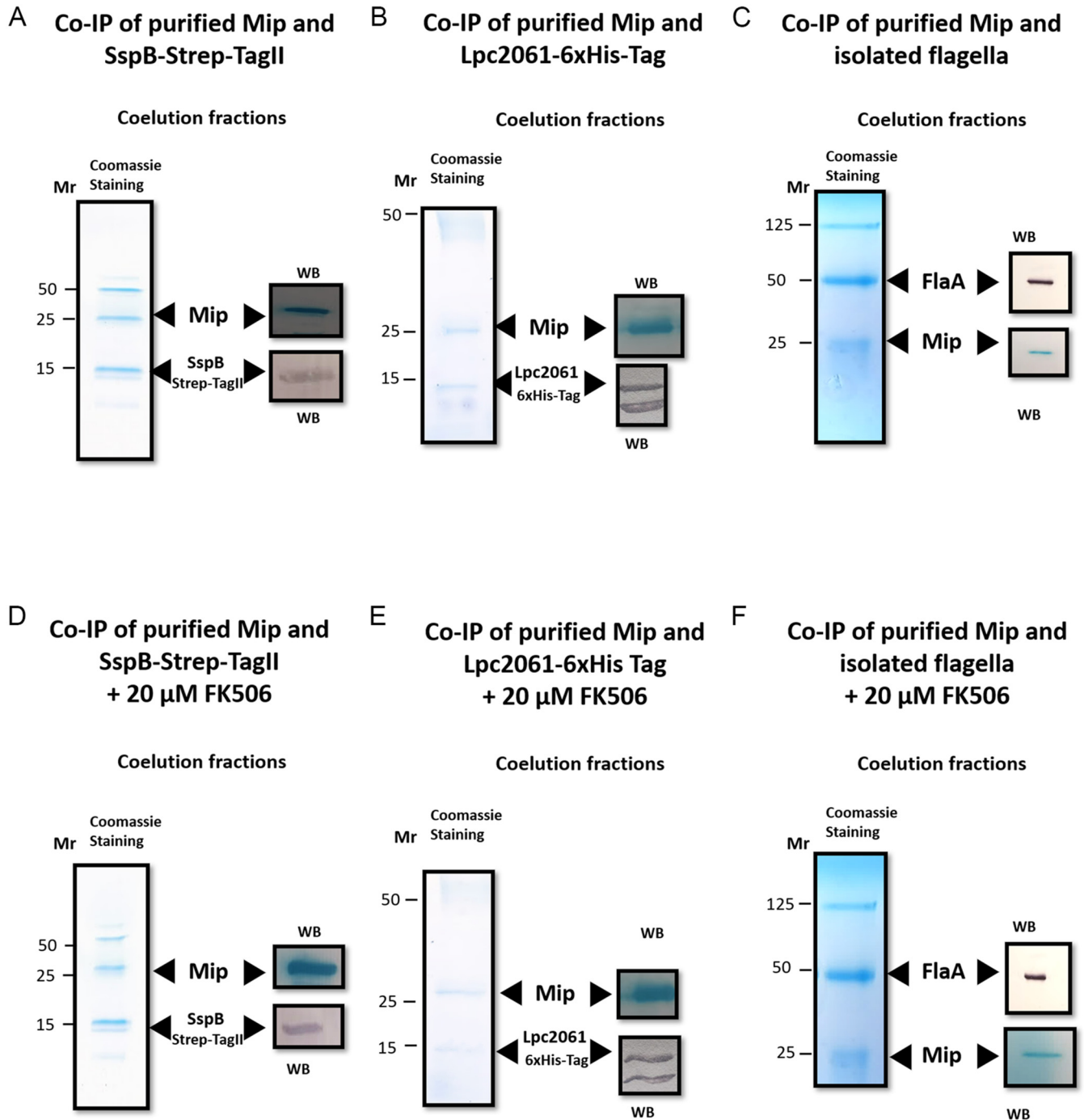


**FIG 2** Validation of Mip interaction partners via the coimmunoprecipitation (CoIP) of SspB-Strep-TagII, Lpc2061-6xHis-Tag, and the purified native flagellin of *L. pneumophila*. Recombinant Mip was immobilized on magnetic DynaBeads coated with Protein G, 2D8, and 22/1 antibodies and was loaded with 1 mg of each purified interaction partner. All coeluates were resolved by SDS-PAGE and Coomassie-stained (left side of panels). The associations of the interaction partners were confirmed by Western-blotting (WB). (A) SspB-Strep-TagII was purified by a Strep-Tactin column. Western blots (WB) with anti-Strep and anti-Mip antibodies confirmed the interaction partners. (B) Lpc2061-6xHis-Tag was purified by a nickel column. Western blots (WB) with anti-6xHis and anti-Mip antibodies confirmed the interaction partners. (C) Coimmunoprecipitation of isolated FlaA and recombinantly produced Mip were confirmed by the anti-FlaA and anti-Mip antibodies. To analyze the influence of FK506 on the coimmunoprecipitation of Mip and the bacterial interaction partners, recombinant Mip was immobilized on magnetic DynaBeads coated with Protein G, 2D8, and 22/1 antibodies, incubated with 20  $\mu$ M PPIase inhibitor FK506, and loaded with 1 mg of the purified interaction partners SspB-Strep-TagII, Lpc2061-6xHis-Tag, or native flagellin from *L. pneumophila*, respectively. (D) The coimmunoprecipitation of recombinantly produced Mip and SspB-Strep-TagII was not influenced by 20  $\mu$ M FK506. Western blots (WB) with anti-Strep and anti-Mip antibodies confirmed the presence of the interaction partners. (E) Addition of 20  $\mu$ M FK506 reduced the coimmunoprecipitation of Mip and Lpc2061-6xHis-Tag. Western blots (WB) with anti-6xHis and anti-Mip antibodies revealed a strong reduction of Lpc2061. (F) The coimmunoprecipitation of recombinantly produced Mip and isolated FlaA was not influenced by 20  $\mu$ M FK506. Western blot (WB) with anti-FlaA and anti-Mip antibodies confirmed the presence of the interaction partners. For the uncropped Western blots, see Fig. S4.

**TABLE 3** Quantification of band intensities from the coelution fractions via ImageJ

Coeluted with Mip	Quantification of antibody signal from Western blot in relative units
SspB-Strep-TagII 15 kDa	5028.832
Lpc2061-6xHis-Tag 15 kDa	4687.276
FlaA 50 kDa	4314.004
SspB-Strep-TagII + 20 $\mu$ M FK506 15 kDa	5181.741
Lpc2061-6xHis-Tag + 20 $\mu$ M FK506 15 kDa	4523.134
FlaA + 20 $\mu$ M FK506 50 kDa	4378.189
Coeluted with Mip	Quantification band intensities in Coomassie stained gels in relative units
SspB-Strep-TagII 15 kDa	4297.674
Lpc2061-6xHis-Tag 15 kDa	1904.648
FlaA 50 kDa	5678.152
SspB-Strep-TagII + 20 $\mu$ M FK506 15kDa	4235.988
Lpc2061-6xHis-Tag + 20 $\mu$ M FK506 15 kDa	794.87
FlaA + 20 $\mu$ M FK506 50 kDa	5743.463
Coeluted with Mip	Quantification band intensity at 15 kDa in Coomassie stained gels in relative units
Flagella + FK506 + Lpc2061	4603.669
Flagella + Lpc2061	7386.962

FK506. Since FK506 binds to the C-terminal binding pocket of Mip (24, 25), this approach also identifies whether or not this pocket is involved in the binding of the identified protein interaction partners. Each of the pulldown assays of the individual partners exhibited both proteins, Mip and the partner, in the eluates (Fig. 2D–F). However, a significant decrease of the hypothetical protein Lpc2061 was detected when the immunosuppressive drug was added (Table 3). These data suggest that the Mip-Lpc2061 interaction requires the C-terminal PPLase domain of Mip.

**The dimerization region and Y185 of Mip are required for the binding of Lpc2061 and FlaA.** To further specify the interaction of Mip with the respective binding partners, we utilized *L. pneumophila* strains expressing Mip variants with single amino acid substitutions or an N-terminally truncated Mip<sup>(77-213)</sup> monomer (Table 1). *L. pneumophila* JR32-2.2 (Mip<sup>(Y185A)</sup> with 2% PPLase activity), JR32-2.3 (Mip<sup>(D142L)</sup> with 6.2% PPLase activity), and JR32-2.4 (monomeric Mip<sup>(77-213)</sup> with 100% PPLase activity) were used (16, 19). All of the versions of Mip are depicted in Fig. 3A. Heterologously-produced, His-tagged Lpc2061 was retained within a nickel-NTA affinity column, which also resulted in additional bands (Fig. S3A), as in the coimmunoprecipitation profile in the cross-linked samples (see Fig. 1B for comparison). Whole-cell extracts derived from the *L. pneumophila* strains expressing the respective Mip variants were incubated with immobilized recombinant Lpc2061. After stringent washing, the coeluates were analyzed by SDS-PAGE and immunodetection using anti-Mip antibodies to monitor the binding of the different Mip variants to Lpc2061 (Fig. 3B–F; Fig. S5A–D). While the Mip<sup>(D142L)</sup> variant, copurified along with Lpc2061, Mip<sup>(77-213)</sup> and Mip<sup>(Y185A)</sup> were unable to bind Lpc2061. Moreover, additional proteins bound to Lpc2061 (besides Mip), and these varied depending upon the Mip variant used (Fig. 3 B–G; Fig. S3A). Wild-type Mip and Mip<sup>(D142L)</sup> showed more intense bands compared to Mip<sup>(Y185A)</sup>, monomeric Mip<sup>(77-213)</sup>, and whole extracts of *L. pneumophila*  $\Delta$ mip, indicating that the Mip-Lpc2061 interaction is responsible for the observed additional protein binding.

Because of the possible colocalization on the cell surfaces of Lpc2061 (predicted with SignalP) (29) and FlaA (30), we also examined a possible Mip:FlaA:Lpc2061 interaction. To assess this, first, whole-cell extracts isolated from the *L. pneumophila* flaA-negative mutant were added to likewise immobilized Lpc2061. In this scenario, Mip was neither detected on the SDS-PAGE nor in the Western blot (Fig. 3G; Fig. S5E). This suggested that FlaA reinforced the Mip-Lpc2061 molecular interaction. In a subsequent experiment, isolated flagella (1 mg/mL) from the *L. pneumophila* wild-type strain were added to immobilized Lpc2061 that was equally incubated with the *L. pneumophila*

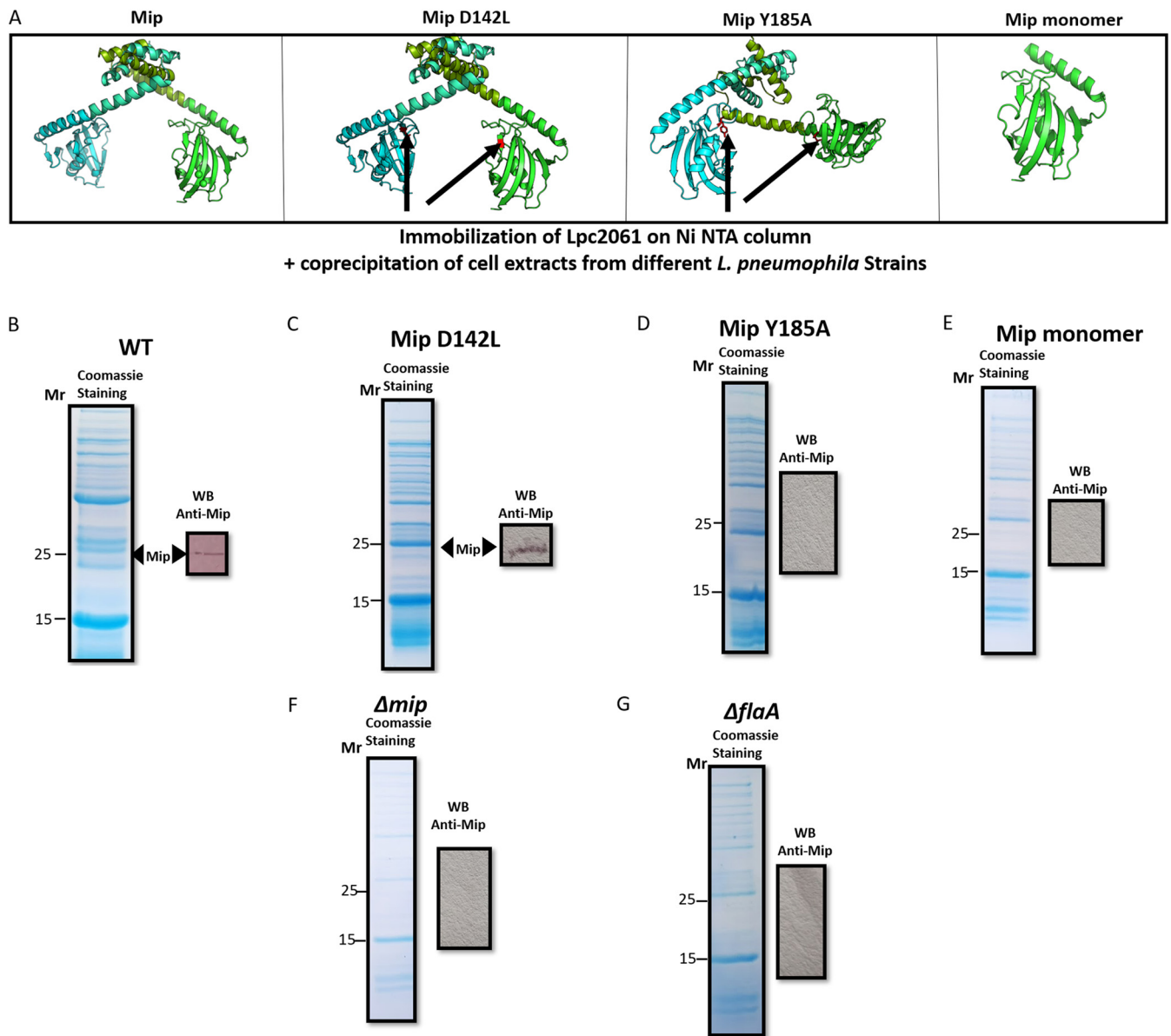


**FIG 3** Coprecipitation of 6xHis-tagged Lpc2061 immobilized on nickel columns and Mip variants with single amino acid substitutions or an N-terminally truncated Mip monomer. (A) The respective structure images of *L. pneumophila* wild-type Mip with 100% PPlase activity, MipD142L with 6.2% PPlase activity, MipY185A with 2% PPlase activity, and monomeric Mip<sup>(77-213)</sup> with 100% PPlase activity were generated using the PyMol tools. Site specific mutations are highlighted in red. Heterologously produced 6xHis-tagged Lpc2061 was incubated with whole-cell extracts from *L. pneumophila* strains expressing the respective Mip variants. Coeluates were analyzed by SDS-PAGE and Coomassie staining. Immunodetection on Western blots (WB) with anti-Mip antibodies were used to determine the binding capacities of the different Mip variants to Lpc2061. (B) Wild-type Mip and (C) Mip D142L were able to bind Lpc2061. (D) Mip Y185A and (E) monomeric Mip<sup>(77-213)</sup> were unable to bind Lpc2061. (F) The whole-cell extract of *L. pneumophila*  $\Delta$ mip was used as a negative-control. (G) Mip was not detected after using whole-cell extracts from *L. pneumophila*  $\Delta$ flaA for coprecipitation, suggesting that FlaA reinforces the Mip-Lpc2061 interaction. For the uncropped Western blots, see Fig. S5.

flaA-negative mutant whole-cell extract, as specified in the previous assay. Consistently, Mip-Lpc2061 coelution was fully restored by adding purified FlaA to the sample (Fig. S5F and G). Due to the observed effect with the *L. pneumophila* flaA-negative mutant, another coimmunoprecipitation was performed by adding both isolated flagella and Lpc2061 protein to immobilized recombinant Mip protein. Mip was coeluted with both of the proteins, and the presence of flagella resulted in an enhanced detection signal of Lpc2061 (Table 3; Fig. S5H-I). The immobilization of SspB resulted in the binding of all tested Mip variants. The SspB-Mip binding was not dependent on FlaA (Fig. S5J). In conclusion, the dimerization region of Mip and amino acid Y185 appear to be crucial for the interaction between

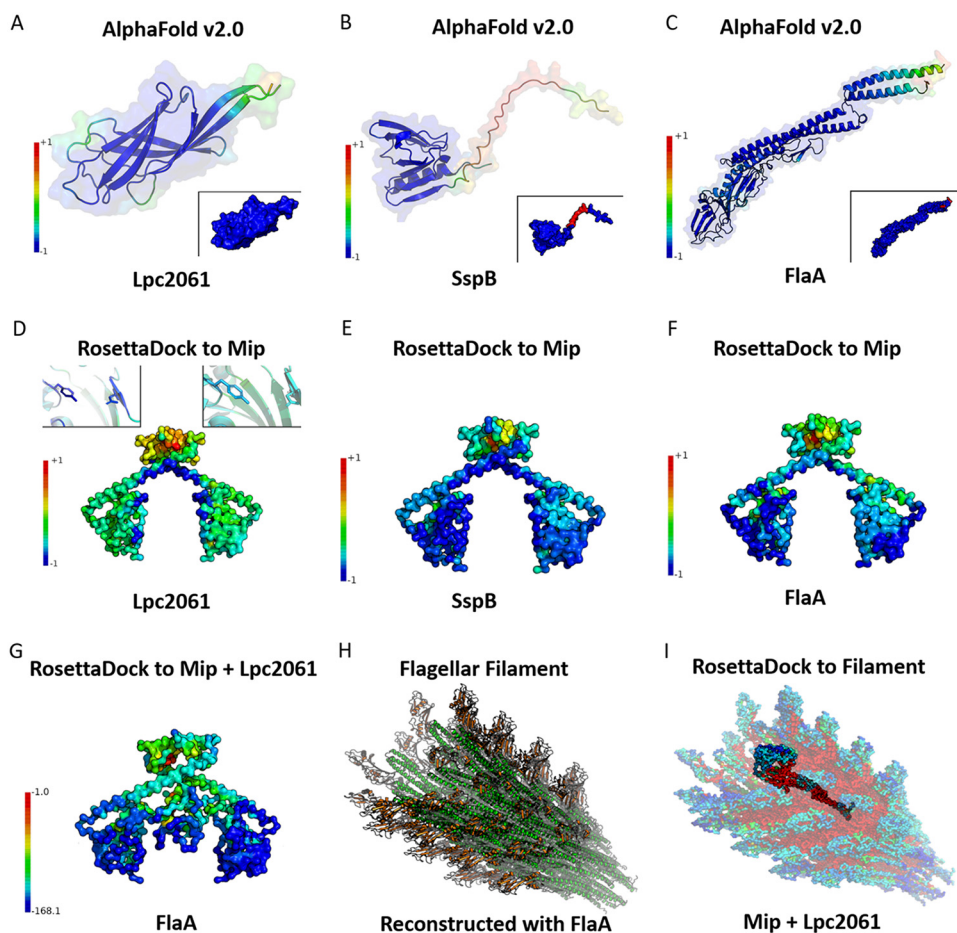


**FIG 4** Modeling of the interaction partners of Mip with AlphaFold v2.0 and of the global docking of each structure to Mip using RosettaDock. The prediction scores were normalized to a range from  $-1$  to  $+1$  (best to worst). The disorder classifications on the protein surface plot are color coded (blue for a strong binding possibility and red for a weak binding possibility). Accordingly, the structure predictions for (A) Lpc2061, (B) SspB, and (C) FlaA are illustrated with color coded modelling scores. The insets show disordered regions, which are classified by pLDDT  $< 50$ . (D) The global docking of Lpc2061, (E) SspB, and (F) FlaA to Mip identifies nonoverlapping binding interfaces. For visualization, the surface of Mip was colored per residue by the interface score of the best poses in which the docking partner has contact. The docking scores were normalized by minimum and maximum values of the respective ensemble in the interval from the best interface score ( $-1$ ) to the worst interface score ( $+1$ ). (G) The docking site of FlaA on a refined version of the best Mip-Lpc2061 pose. The normalized interface score is color coded on Mip-Lpc2061. To better visualize the difference an exponential scaling law  $-e^{-0.1 \cdot I_{sc}}$  was applied to the interface score. (H) Flagellar filament reconstructed from the FlaA structure prediction and the Cryo-EM structure of *P. aeruginosa* flagellar filaments (PDB ID: 5WK6). *L. pneumophila* specific FlaA regions unresolved in the Cryo-EM structure are highlighted in orange. (I) Global docking of the modeled flagellar filament surface, Mip, and Lpc2061.

Lpc2061 and Mip, which is strengthened by FlaA, while the binding of SspB to Mip occurred, irrespective of the tested variant, and was not affected by the presence of FlaA.

**Modeling of interaction partners and global docking with Mip suggests nonoverlapping binding interfaces.** As no experimentally determined complete structures exist for the identified interaction partners, we predicted these *in silico* using AlphaFold v2.0 (Fig. 4). The predicted structure of Lpc2061 consists of  $\beta$ -sheets connected by loop regions, with a good score, overall (normalized score around 0), except for some surface loop regions (amino acids 16 to 21 and 49 to 54) as well as the N and C termini (Fig. 4A). The inset of Fig. 4A shows that there is likely no disorder in this structure. The SspB model, according to AlphaFold v2.0, shows a structure that is similar to the resolved parts of the *E. coli* SspB 1TWB (31) (Fig. 4B). The tail-like structure of *L. pneumophila* SspB harbors a region that is classified as disordered (inset of Fig. 4B). FlaA is predicted to be a long protein which can be separated into a complex region that contains  $\alpha$ -helices as well as  $\beta$ -sheets and loops as well as a long domain that primarily contains  $\alpha$ -helices

(Fig. 4C). The only regions classified as possibly disordered are small regions at the N and C termini (inset of Fig. 4C).

To develop a hypothetical model for the three interaction partners, we ran global docking simulations with Mip (Fig. 4D and E). Unanimously, the worst overall docking scores are located in the upper part of the Mip dimerization region. For Lpc2061, the best scoring regions are inward of the C-terminal PPlase domain and at the basis of the  $\alpha$ -helix above the dimerization region (Fig. 4D). Furthermore, there was a visible difference in the interface scores of the residues Asp142 and Tyr185 in each PPlase domain. The normalized interface on the left PPlase domain was  $-0.79$  for Asp142 and  $-0.98$  for Tyr185, whereas it was  $-0.4$  for Asp142 and  $-0.59$  for Tyr185 on the right PPlase domain. For SspB, there seems to be no clear optimal area standing out from the ensemble. Mostly, both PPlase domains of Mip showed a low interface score, which suggests that this protein has no specific binding site for SspB (Fig. 5E). For FlaA (Fig. 5F), the region containing the lowest interface score was located more on the outward facing part of the PPlase domain (residues 96 to 106). Residues 107 to 212 of Mip, on the other hand, are closer to the long  $\alpha$ -helices (residues 55 to 96), which connect the PPlase regions with the dimerization interface of the homodimer. Since the putatively best binding region for FlaA is at a different nonoverlapping location, compared to the low interface score region identified for Lpc2061, both score distributions seem to be complementary. This is in accordance with the observation that FlaA reinforces the Mip-Lpc2061 interaction. This tripartite interaction was modeled by docking FlaA to the refined best pose of the Mip-Lpc2061 interaction. As illustrated by the color code of the normalized interfaces after applying the exponential scaling law  $e^{-0.1 \times L^{5C}}$  (32, 33) to better visualize the differences (Fig. 4G), the tripartite ensemble shows similar regions of the most negative scores compared to the respective single interactions. The complete histograms of the docking interface scores of Lpc2061, SspB, and FlaA, as well as those of the whole ensemble (Mip with Lpc2061 and FlaA) further illustrates this view (Fig. S6).

For a further interpretation of our data set, we also modeled the flagellar filament by fitting multiple copies of the predicted *L. pneumophila* FlaA structure into the near-atomic resolution cryo-EM structure (PDB ID: 5WK6) of *Pseudomonas aeruginosa* PAO1 (34). The reconstructed filament structure is illustrated in Fig. 4H, in which the *L. pneumophila* specific regions of FlaA are highlighted. Via the global docking of the modeled filament surface, Mip and Lpc2061, we generated 8,000 poses (Fig. 4I). The best pose of FlaA, Mip, and Lpc2061 in this filament is consistent with the global docking of the tripartite interactions, independent of the filament context. Moreover, the *L. pneumophila* specific regions in the filament revealed the best binding interfaces (lowest scores) for binding Mip and Lpc2061.

**Molecular dynamic simulations predict increased stability for the tripartite interaction of Lpc2061, Mip, and FlaA.** Based on our biochemical results, we further hypothesized that the tripartite interaction of Lpc2061, Mip, and FlaA entails increased stability. Molecular dynamics (MD) simulations starting from the refined docking of the best global poses with Mip are illustrated in Fig. 5. For the entire structures of SspB, Lpc2061, FlaA, and Lpc2061 with FlaA, respectively, the overall RMSD were plotted over a simulation time of 500 ns (Fig. 5A and B). The interface RMSD (i-RMSD) and contacts for the interface atoms of the respective Mip-interaction partners were similarly plotted over the simulation time (Fig. 5C–F). The RMSDs of the overall simulations were used to evaluate the stability of the observed dynamics. Simulations for Mip interacting with SspB or Lpc2061 revealed a relatively stable interaction, since a horizontal line with relatively little perturbations represents a largely constant value (Fig. 5A). The simulations of FlaA or Lpc2061 with FlaA exhibited far more deviations (Fig. 5B). FlaA alone was unstable between 300 ns and 450 ns, and the addition of Lpc2061 to FlaA showed increased stability after 200 ns, although fluctuations still occurred. A similar trend was observed with i-RMSD, with which the Mip-FlaA interface score exhibited more and higher peaks compared to the Mip-FlaA interface score when Lpc2061 was added (Fig. 5C). The i-RMSD of the Mip-SspB interface revealed a higher stability compared to the Mip-Lpc2061 interface. However, the stability of the Mip-Lpc2061 was increased by the addition of FlaA and was then on a similar level as the Mip-SspB

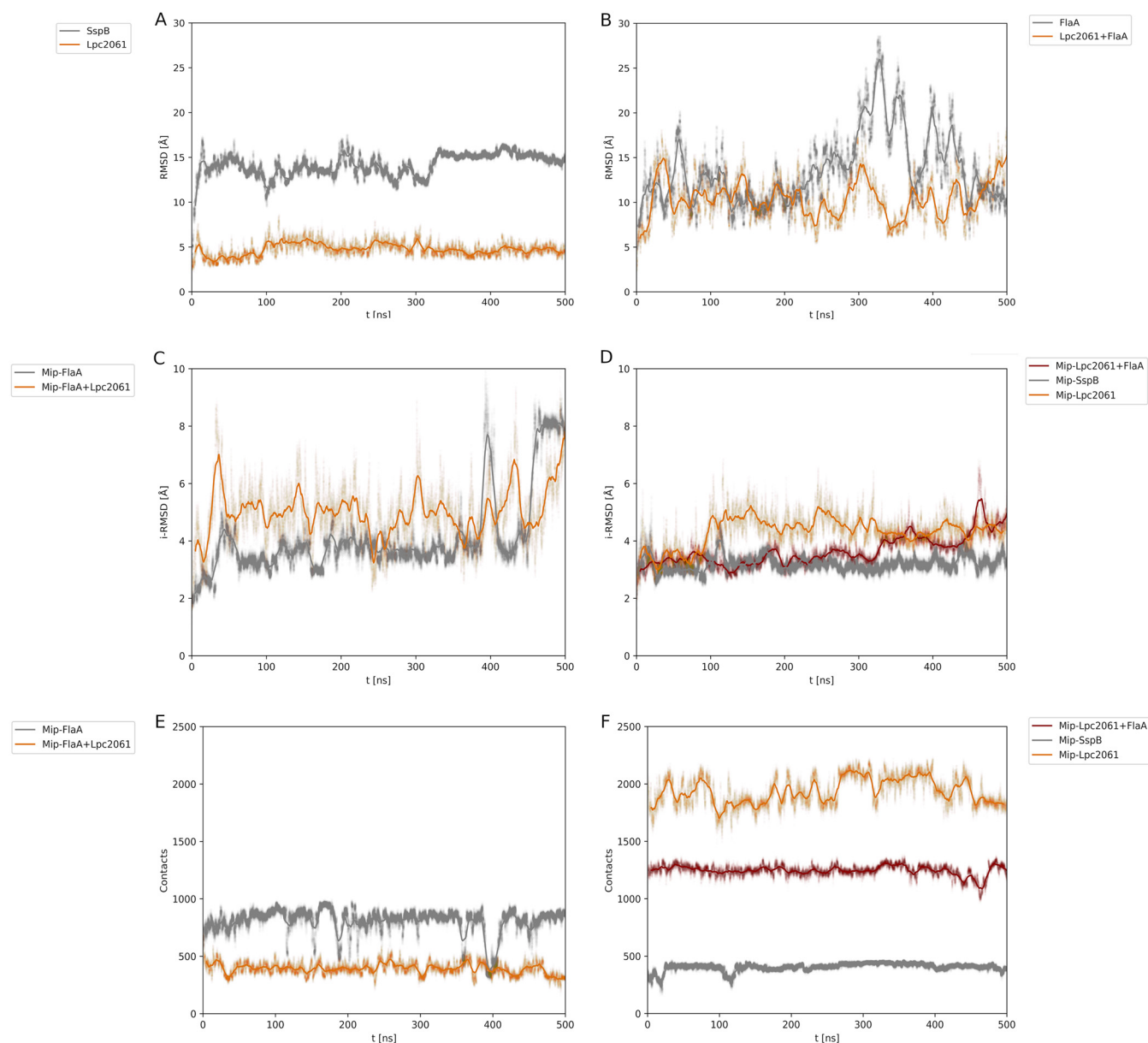


**FIG 5** MD simulations of the best global poses of SspB, Lpc2061, and FlaA with Mip. The RMSDs were plotted over a simulation time of 500 ns and (A) revealed a stable interaction for SspB and Lpc2061. (B) Simulations for FlaA and Lpc2061 with FlaA, respectively, revealed strong deviations. However, the addition of Lpc2061 reduced the fluctuations. (C) The iRMSD of the Mip-FlaA interface score exhibited higher peaks, and these were not reduced by the addition of Lpc2061. (D) The stability of Mip-Lpc2061 was increased by the addition of FlaA and remained on a similar level to that of the Mip-SspB interface. (E) The number of contacts, defined as a 10 Å vicinity of atoms within the protein-protein interface, between Mip and FlaA over the duration of the simulation decreased when Lpc2061 was added. (F) Mip-SspB showed the fewest contacts, followed by Mip-Lpc2061 plus FlaA and Mip-Lpc2061.

interface (Fig. 5D). Interestingly, the absolute number of contacts between Mip and FlaA over simulation time decreased when Lpc2061 was added (Fig. 5E). Mip-SspB showed the fewest contacts, followed by Mip-Lpc2061 plus FlaA and Mip-Lpc2061 (Fig. 5F). Nevertheless, the tripartite interaction appeared more stable, as large peaks were absent. All four simulations are illustrated in Supplemental Movies M1–M4. The minimum RMSD between each pose from the flagellar filament and the MD trajectory for Mip-Lpc2061 plus FlaA scattered around the interface score are illustrated in Fig. S7. The interaction of Lpc2061, however, seems to be stable, judging from both the overall as well as the interface RMSD values. This is also visible during the 500 ns trajectory, as visualized in Supplemental Movie M1. Moreover, there is almost no deviation from the positioning of Lpc2061 between the two PPIase domains. The best pose was identical

with the lowest RMSD in the trajectory. This is also illustrated in Supplemental Movies M5–M8, in which the MD trajectory is superimposed on the best poses of FlaA.

**Mip promotes flagellation and the yield of *L. pneumophila* FlaA.** As published previously, the formation of intact flagella correlates with the flagellin expression of *L. pneumophila* (35). To analyze whether Mip impacts bacterial motility, we first inspected *L. pneumophila* cells expressing wild-type Mip and Mip variants with single amino acid substitutions and the N-terminally truncated Mip monomer via phase-contrast microscopy. The *L. pneumophila*  $\Delta flaA$  mutant, which is unable to produce FlaA or flagella, was used as a negative-control. This approach revealed that the motility of the *L. pneumophila*  $\Delta mip$  mutant and cells expressing the monomeric Mip<sup>(77-213)</sup>, or Mip<sup>(Y185A)</sup> was impaired (Movie movS9–movS13). The strain expressing Mip<sup>(D142L)</sup> with 6.2% PPlase activity showed a slightly reduced motility compared to the *L. pneumophila* wild-type strain (Movie movS14).

Since the monopolar flagella of *L. pneumophila* cells easily break under shear forces, which causes difficulties in quantifying them via TEM, we isolated flagella from equal amounts of biomass of the *L. pneumophila* wild-type strain and mutants (Fig. 6A & B). The TEM revealed intact flagella in preparations from the *L. pneumophila* wild-type strain and, to a much lesser extent, in the isogenic  $\Delta mip$  mutant. Preparations from the  $\Delta flaA$  mutant were completely devoid of flagellar structures. Preparations from *L. pneumophila* mutants expressing Mip-variants with reduced PPlase-activity or the N-terminally truncated Mip monomer also exhibited fewer flagellar structures, compared to the wild-type strain. Subsequent quantification of the 50 kDa FlaA protein by SDS-PAGE, Coomassie-staining, and ImageJ confirmed this observation (Fig. 6C). Again the *L. pneumophila*  $\Delta flaA$  mutant was used as a negative-control, and the faint band intensity of 4031.3 units that resulted from the preparation of this mutant was taken as the background. The band intensities of the Coomassie-stained SDS gels revealed that the signal of FlaA extracted from the *L. pneumophila* wild-type strain was 10,589 units (Fig. 6C and Fig. S8). Strikingly, the flagellar preparations from the *mip*-negative mutant resulted in a band intensity of 1,889 units, a 5.6-fold decrease compared to that of the wild-type strain. The site-specific mutant expressing the Mip<sup>(D142L)</sup>-variant with 6.2% PPlase activity exhibited a significantly higher band intensity in Coomassie-stained SDS gels and a higher FlaA concentration ( $\mu\text{g}/\text{mL}$ ) compared to the strains expressing Mip<sup>(Y185A)</sup> (with 2% PPlase activity) or the monomeric Mip<sup>(77-213)</sup> (with 100% PPlase activity) (Fig. 6C; Table S1 and S2). Similarly, treating *L. pneumophila* with 20  $\mu\text{M}$  FK506 resulted in a lower FlaA yield (Fig. 6D; Table S3 and S4).

## DISCUSSION

PPlases of pathogens are involved in a broad spectrum of phenotypes, including virulence, metabolism, and multiple stress responses (36–42). Likewise, the PPlase Mip of *L. pneumophila* contributes to infection, collagen binding, phospholipase C-like activity, transmigration across tissue barriers, nematode colonization, surface translocation, and growth at suboptimal temperature (28, 43–45). Mip targeting antimicrobial inhibitors, such as cycloheximide, pipercolic acid, and FK506 derivatives further corroborated the observation of the moonlighting activities of Mip in the fundamental processes of infection (39, 46–50). Nevertheless, the natural substrates and specific molecular activities of Mip remain largely elusive.

Here, we present for the first time the identification of bacterial interaction partners of *L. pneumophila* Mip. Immunoprecipitation revealed SspB (LPC\_0434) as an *in vivo* interaction partner of Mip. Cross-linking with FA additionally identified the hypothetical protein Lpc2061 and the main flagellar monomer FlaA (LPC\_0756) as interaction partners. The SspB homologues (e.g., those in *E. coli* [52% identity] and *Pseudoalteromonas* spp. [62% identity]) are well-known dimeric adaptor proteins which increase the rate at which *ssrA*-tagged substrates are degraded by tethering them to the ClpXP protease (51, 52). Interestingly, the SspB of *Salmonella enterica* serovar Typhimurium, which, like *L. pneumophila*, has no secretion signal, has been found in bacterial culture supernatants and is inserted into host cell plasma membranes shortly after bacterial infection (53). The ClpXP protease of this pathogen negatively regulates flagellar synthesis. The respective

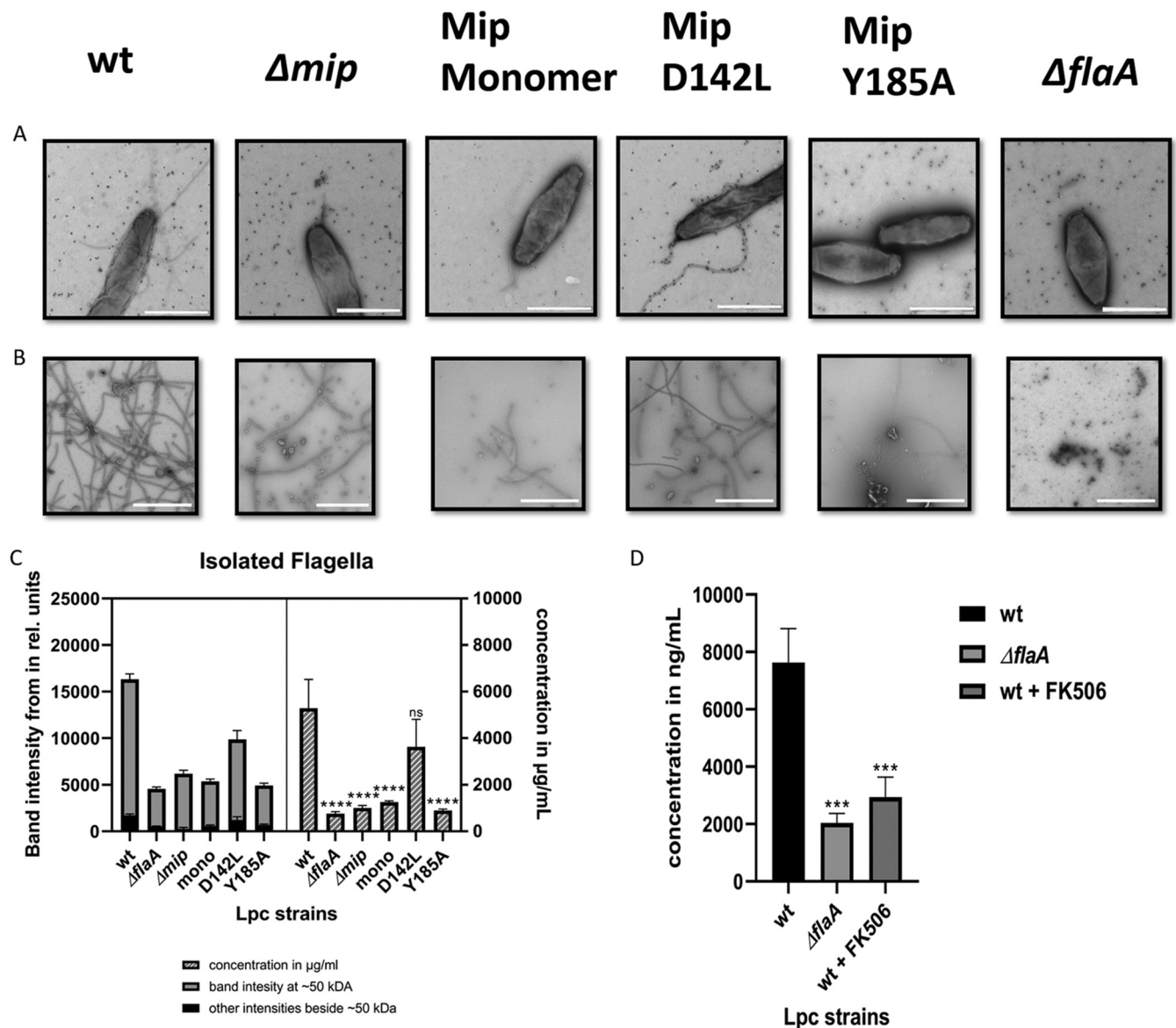


**FIG 6** Impact of Mip on the bacterial flagellation and the quantification of FlaA. (A) TEM of isolated flagella from equal amounts of biomass of the *L. pneumophila* wild-type, the  $\Delta mip$  mutant, and strains expressing the N-terminally truncated Mip monomer and Mip variants with single amino acid substitutions (Mip D142L, Mip Y185A). The *L. pneumophila*  $\Delta flaA$  mutant, which is unable to produce FlaA or flagella, was used as a negative control. Size: bar = 1  $\mu\text{m}$ . (B) TEM of flagella isolated from  $10^{14}$  bacteria of the respective *L. pneumophila* wild-type strain and mutants. (C) Quantifications of FlaA from Coomassie stained SDS gels (band  $\sim 50$  kDa) were performed by using the ImageJ band intensity determination tools and Roti Nanoquant at 590 nm/450 nm. The identity of FlaA was confirmed by Western blotting (Fig. S8). *L. pneumophila*  $\Delta flaA$  was used as a negative-control and was taken as the background for the quantification of FlaA. (D) Comparison of flagellar preparations from  $10^{11}$  bacterial cells of the *L. pneumophila* wild-type, the  $\Delta flaA$  mutant, and the wild-type treated with 20  $\mu\text{M}$  FK506. Three replicates were compared via Dunnett's multiple-comparison test. \*\*,  $P < 0.01$ ; \*\*\*,  $P < 0.001$ ; \*\*\*\*,  $P < 0.0001$ ; ns, not significant.

ClpXP deletion mutants exhibit overproduction of the flagellar protein, a 4-fold increase in the rate of transcription of *fliC*, and a hyperflagellated phenotype (54). Whether Mip intercepts SspB and by this means downregulates the ClpXP-dependent repression of the flagellar regulon in *L. pneumophila* has yet to be shown. The hypothetical protein Lpc2061 shows structural homology to glycoside hydrolases; however, its actual function remains unclear. *L. pneumophila* FlaA is the major component of the surface exposed flagellar filament. Like SspB, FlaA is expressed during starvation periods in the postexponential phase of *L. pneumophila* (30).

The interactions with Mip were validated via a complementary approach using the tagged variants of SspB and Lpc2061 as well as purified native *L. pneumophila* FlaA.

Moreover, the respective binding strengths, with SspB as the strongest, followed by Lpc2061 and FlaA, were semiquantified by determining the band intensities of Western blots. Since the PPlase activity of Mip is inhibited by FK506 (23), and since this macrolide decreased the coimmunoprecipitation of the hypothetical protein Lpc2061 and the binding between Mip and SspB was not affected by point mutations which reduce the PPlase activity, we conclude that the C-terminal PPlase domain of Mip is involved in the binding of Lpc2061. As several of the virulence and fitness functions of Mip are not related to enzymatic catalysis, but rather to moonlighting activities in the host (28, 47, 48), it is unsurprising that not all of the interactions were negatively influenced by FK506. Further characterization of the interactions by *L. pneumophila* strains expressing Mip variants with single amino acid substitutions or N-terminally truncated monomers revealed that the dimerization region and the amino acid Y185 of Mip are essential for the binding of Lpc2061, whereas these regions are not required for SspB binding. Previous studies already revealed that, mediated by a hinge in the long  $\alpha$ -helix, both of the PPlase domains of dimerized Mip are subject to large fluctuating movements, allowing for the flexible cooperative binding of potential target structures (25). To what extent this applies to Lpc2061 remains to be clarified.

Interestingly, FlaA reinforced the Mip-Lpc2061 interaction, as adding isolated FlaA restored the coelution of Mip-Lpc2061 from a *L. pneumophila* flaA-negative mutant. This effect of FlaA was not observed for the Mip-SspB interaction. These experimental findings are in good agreement with computational modeling of the interaction partners and the global docking with Mip, since the putatively best binding region of FlaA shows no overlap with the binding interface of Lpc2061. Although the combination of 3D structure prediction and docking has a limited accuracy, MD simulations suggest an increased stability for the tripartite interaction of the Lpc2061-Mip-FlaA ensemble. Except for SspB, which could be coimmunoprecipitated without FA cross-linking and revealed the highest binding strength, a far-reaching consistency of our biochemical data and computational predictions regarding the stability of the interaction partners was observed. According to the best poses (docking), our computational data (MD) suggest that the interactions Mip-Lpc2061, Mip-SspB, Mip-FlaA, and Mip-Lpc2061-FlaA are stable. For the Mip-Lpc2061 interface in the tripartite complex, we see a lower i-RMSD. Also, the fluctuations in the number of contacts are less in the tripartite complex compared to the Mip-Lpc2061 interaction. This indicates that the Mip-Lpc2061 interface in the tripartite complex is more stable than the Mip-Lpc2061 binary interaction. Since SspB showed no outstanding specific binding area in the global docking with Mip (which is consistent with our biochemical data) and molecular dynamics simulations using the best pose with Mip, the discrepancy regarding the best binder can be explained. Overall, the results from biochemical assays, modeling, docking, and dynamic simulations are consistent, help to portray the putative binding interfaces, and suggest an increased stability for the tripartite interaction of the ensemble of Mip, Lpc2061, and FlaA.

To better understand the functional implications of the observed protein interactions and the hypotheses deduced from the computational biology, we microscopically analyzed flagellar preparations of the *L. pneumophila* wild-type strain, the isogenic  $\Delta mip$  mutant, and the *L. pneumophila* strains producing Mip variants with single amino acid substitutions or N-terminally truncated monomers of Mip. Moreover, we quantified FlaA preparations of these strains. We clearly demonstrated that wild-type Mip promotes the flagellation of *L. pneumophila* and the yield of FlaA. Interestingly, all of the *L. pneumophila* strains that were expressing Mip variants were significantly less flagellated compared to the wild-type strain. In accordance with the biochemical results showing that FlaA and Lpc2061 mutually reinforce their binding to Mip, which was also suggested by the MD simulations, we observed that the binding regions of Mip in the Mip-Lpc2061 interaction positively influences flagellation. The *L. pneumophila* mutants expressing the Mip<sup>(Y185A)</sup> or the monomeric Mip<sup>(77-213)</sup> variant, which bind less Lpc2061, were less flagellated and yielded less FlaA. Also, FK506 treatment

resulted in a lower FlaA yield. Thus, we propose a model in which Mip in concert with Lpc2061 is important for *L. pneumophila* flagellation.

In *L. pneumophila*, the expression of a single monopolar flagellum is life cycle-dependent and correlates with the virulent postexponential growth phase. The pathogen is not flagellated during intracellular replication but becomes so during the transmissive phase, when it lyses its spent host and searches for a new replication niche (55). Then, like Mip, the major subunit FlaA positively affects the early phase of infection of eukaryotic host cells (35), as the non-flagellated mutants of *L. pneumophila* are less infective for amoebas and macrophages (35, 56). Moreover, FlaA mediates the toxicity to host cells (30, 57). We hypothesize that certain effects of Mip or FlaA on *L. pneumophila* pathogenicity are mediated or regulated by their interaction. It is even imaginable that Mip assists in the flagellar assembly or regulation, as is suggested by our flagellation assays. Interestingly, monomeric FlaA induces innate the immunity of alveolar macrophages and lung epithelial cells (30). The globular domain D<sub>1</sub> and the D<sub>0</sub> polymerization domain of FlaA are recognized by TLR5, which plays an important role during bacterial clearance (58, 59). Accordingly, a tight control of flagellation and an extracellular release of FlaA appear to be critical for the environmental fitness and pathogenicity of *L. pneumophila*.

To the best of our knowledge, this is the first report in which a bacterial PPLase was demonstrated to influence flagellation. Our results revealed Mip as a binding partner of FlaA and as an amplifier of *L. pneumophila* flagellation. Our results point toward a positive modulation of this phenotype by the Mip interaction partner Lpc2061, a protein of yet unknown function. Moreover, starvation signals are also known to play a role in the flagellar regulon via ppGpp (30). Whether or not (and if yes, in which way) the Mip binding partner SspB is also involved in this interaction remains elusive and should be addressed in further studies.

## MATERIALS AND METHODS

**Bacterial strains and culture.** *L. pneumophila* strains were grown either on Buffered Charcoal Yeast Extract (BCYE) agar (10 g/L yeast extract and 10 g/L ACES (N-(2-Acetamido)-2-aminoethanesulfonic acid) buffer [pH 6.9] supplemented with 0.4 g/L L-cysteine, 0.25 g/L iron (III) nitrate, and 15 g/L agar) or in Buffered Yeast Extract (YEB) medium (10 g/L yeast extract, 10 g/L ACES buffer [pH 6.9] supplemented with 0.4 g/L L-cysteine and 0.25 g/L iron (III) pyrophosphate). Luria-Bertani (LB) medium (5 g/L yeast extract, 10 g/L peptone, 5 g/L NaCl) was used for culturing the *E. coli* strains. When required, antibiotics or FK506 were added to the following final concentrations: 20 μg/mL kanamycin, 12.5 μg/mL chloramphenicol, 50 μg/mL streptomycin, and 20 μM FK506 for *L. pneumophila* and 100 μg/mL ampicillin for *E. coli*. The bacterial strains and primers employed throughout this work are listed in Table 1.

**In vivo cross-linking and cell fractionation of *L. pneumophila*.** *L. pneumophila* was grown in 1 L YEB to an OD<sub>600</sub> (optical density) of 1.8. Different concentrations of formaldehyde (vol/vol) were added to the culture medium: 0%, 0.25%, 0.5%, 0.75%, and 1%. formaldehyde (FA) was allowed to penetrate bacterial membranes and elicit cross-linking reactions for 30 min at 37°C with shaking at 200 rpm. The reactions were quenched with 130 mM glycine for 5 min at 200 rpm. After this, the cells were harvested by centrifugation at 4,000 × g for 20 min at 4°C. From here on, the protocol was carried out at 4°C. The pellet was resuspended in suspension/lysis buffer (100 mM Tris-HCl [pH 7.5], 150 mM NaCl, 1 mM EDTA). A tablet of protease cocktail inhibitor (Roche) was added per 10 mL volume. Bacteria were subsequently homogenized with FastPrep (MP Biomedicals FastPrep-24) (two times, 6 m/s for 30 s). Centrifugation at 4,000 × g for 20 min followed in order to eliminate cell debris. The supernatants were ultracentrifuged for 1 h at 100,000 × g. Subsequently, the insoluble fraction was dissolved in PBS-buffer supplemented with 1.8% (vol/vol) Triton X-100 overnight at 4°C under continuous rotation. Thereafter, the solubilized mix was centrifuged at 16,000 × g for 20 min, and soluble fractions were harvested. The isolated protein fractions were immunoprecipitated (see "Immunoprecipitation of Mip and analysis of binding domains"), separated by SDS gel electrophoresis, and stained and/or transferred for Western blotting (60).

**Recombinant protein production.** The genes of the putative interaction partners *lpc2061* and *lpc0434* (SspB) were amplified from the *L. pneumophila* genome using the primers specified in Table 1. All primers contained restriction sites as overhangs. *lpc2061* and *lpc0434* were treated with corresponding restriction enzymes and ligated into the equally treated expression vectors pET-22b(+) (Novagen 69744-3) or pET-52b(+) (Novagen 71554), respectively. The resulting constructs were named p2061-His and pSspB-Strep. Plasmids were introduced into chemically competent *E. coli* BL21 cells (61). This led to the construction of the recombinant strains BL21-pet22b-*lpc2061* and BL21-pet52b-*sspb*. The most suitable conditions for Lpc2061-6×His-Tag production turned out to be 1 μM IPTG induction and incubation at 17°C overnight. Recombinant SspB-Strep-TagII production was successful upon induction with 1 μM IPTG and incubation at 37°C for 6 h. The bacteria were harvested and washed twice with PBS (4,000 × g for 20 min at 4°C). Thereafter, the pellets were resuspended in 20 mL PBS supplemented with 1 tablet of protease inhibitor cocktail (Roche), wherein 10 mM imidazole was added to the buffer for

Lpc2061. Then, the mixture was processed with a FrenchPress (ThermoFisher FA-032) and centrifuged again at  $4,000 \times g$  for 20 min at 4°C. The supernatants were filtered through a  $0.45 \mu\text{m}$  filter, and the resulting extracts were applied to a nickel-NTA column (Macherey-Nagel number 745415.5) or a StrepTactin column (Iba Life Sciences number 2-5998-000) for Lpc2061 and SspB, respectively. Purification was performed as specified by the manufacturers. Flowthrough, wash, and elution fractions were collected for further analyses via SDS gel electrophoresis and Western blotting.

**Native isolation of flagella.** *L. pneumophila* strains were grown in YEB medium overnight, and 200  $\mu\text{L}$  of cultures were plated on BCYE agar. The BCYE plates were incubated at 30°C for 5 days, and  $10^{11}$  (for the inhibitor experiments) and  $10^{14}$  bacteria (for the Mip variant experiments) were resuspended in 20 mL PBS. The suspensions were then blended with a homogenizer (Polytron PT2500 E) for 3 min. Centrifugation was subsequently performed at  $16,000 \times g$  for 15 min at 4°C. The supernatants were withdrawn and centrifuged again at  $40,000 \times g$  for 3 h at 4°C. The resulting pellets were pulled out and resuspended in a 5 mL final volume of phosphate buffer, and isolates were diluted to 2 mg/mL total protein content (62). The isolation of flagella from equal amounts of bacteria ( $10^{11}$  or  $10^{14}$  bacteria) were performed in duplicate and repeated 3 times. The concentrations were measured with a Roti Nanoquant (Carl Roth GmbH + Co., KG number K880) and determined according to OD at 590/450 nm. The purities of the flagella preparations were confirmed spectrophotometrically using a Nanodrop Implen NanoPhotometer N50 at 260/280 nm.

**Immunoprecipitation of Mip and analysis of binding domains.** To immunoprecipitate Mip, DynaBeads (Thermo, number 10003D) were coupled with 22/1 and 2D8 monoclonal mouse antibodies (63). *L. pneumophila* were grown in liquid culture and homogenized using FastPrep. When the solubilization of the membrane fractions was required, 1.8% (vol/vol) of Triton X-100 was added as described in "In vivo cross-linking and cell fractionation of *L. pneumophila*" (60). The resulting solubilized membranes were incubated with DynaBeads for the immobilization and purification of Mip from membrane fractions (28 kDa) or the respective variants. When required, 1 mg of recombinant or native proteins (see "Recombinant protein production" and "Native isolation of flagella") were added to Mip immobilized on DynaBeads and were harvested as described above. Alternatively, recombinantly produced Mip (25 kDa) was used for coprecipitation procedures (15). The influence of FK506 (Sigma-Aldrich F4679) on interactions between Mip and the protein partners was analyzed by adding 20  $\mu\text{M}$  PPIase inhibitor to DynaBeads-bound recombinant Mip (15). All of the coeluates, including the flowthrough and wash fractions (purity control) were resolved on a 15% acrylamide SDS-PAGE. The gels were Coomassie-stained (100 g/L  $(\text{NH}_4)_2\text{SO}_4$ , 100 mL/L  $\text{H}_3\text{PO}_4$ , 20% [vol/vol] methanol) overnight, as described previously (64). Silver staining of the gels was also performed as described previously (65). Mip was detected employing rabbit anti-Mip polyclonal antibodies as specified elsewhere (66). In brief, proteins were transferred onto a PVDF-membrane via semidry blotting (5 min, 1.3 mA, and 25 V). The membranes were blocked with TBST (0.2% [vol/vol] Tween 20) containing 3% (wt/vol) low fat milk powder. Subsequently, TBST with 1% (wt/vol) milk powder, including the primary antibodies (1:10,000) for Mip (66) and FlaA detection (67) and the anti-Strep (Iba Lifescience Strep-Tactin AP conjugate 2-1503-001) and anti-His (Invitrogen 6 $\times$ -His Tag Monoclonal Antibody) antibodies for the detection of SspB and Lpc2061, respectively, were used. Secondary mouse or rabbit antibodies were added at 1:10,000 dilution in 1% (v/w) TBST milk powder. Chromogenic reactions by which to visualize the respective proteins were carried out by adding 0.66% (vol/vol) Nitro Blue Tetrazolium (NBT) and 0.33% (vol/vol) 5-bromo-4-chloro-3-indolyl phosphate (BCIP). The quantification of proteins was performed using the ImageJ band intensity determination tools. The quantification reflects the relative amounts as a ratio of each protein band, relative to the lane's loading control. For the LC-MS/MS analysis, the samples were migrated 10 cm into a SDS-PAGE and stained with Coomassie. The bulky band was excised with a scalpel and shipped to Proteome Factory AG for further analyses using a Thermo Scientific LTQ Orbitrap XL hybrid FTMS device in a medium gradient (see <https://www.proteome-factory.com/> for further details).

**Motility and transmission electron microscopy of isolated flagella.** The motility of *L. pneumophila* strains and mutants was scored qualitatively by examining wet mounts of *L. pneumophila* broth cultures via phase-contrast microscopy at a magnification of 320 $\times$ . A culture (stationary-phase) was defined as motile if at least half of the bacteria in a field of at least 100 cells were judged to exhibit rapid, directed movement. Movies of motile and nonmotile bacteria were recorded at a magnification of 320 $\times$  using an Oppo-Find-X5-Pro Android camera. Flagella samples were prepared as described in "Native isolation of flagella," and 200  $\mu\text{L}$  aliquots were used for negative staining. A thin carbon film was floated on sample droplets (approximately 30 to 40  $\mu\text{L}$ ) to allow for the adhesion of flagella. After 1 min, a 300 mesh copper grid was placed on the film to take it off. The filmed grid was washed twice with distilled water and incubated for 1 min on a droplet of 4% (wt/vol) uranylacetate, and this was followed by the removal of excessive liquids and drying. Electron microscopy was performed with a Libra 120 Plus (Zeiss, Germany) at an acceleration voltage of 120 kV and with calibrated magnifications using the WinTEM/ITEM software package.

**Modeling of proteins with AlphaFold v2.0.** To predict the structures of the potential Mip-interaction partners, Lpc2061, SspB, and FlaA, the standalone version of AlphaFold v2.0 (<https://alphafold.ebi.ac.uk/>) in monomer mode was used (68). The visualization of quality and the final ranking of the model were achieved via the local difference test (pLDDT)-scoring, which is based on the  $C\alpha$  positions (68). Since a pLDDT score of  $<50$  is associated with disordered regions (68), this classifier was evaluated for the final predictions. For visualization, the prediction score was normalized on a range from  $-1$  to  $+1$  (best to worst). The results of the disorder classification were then visualized on the protein surface plot in the according insets with blue for no disorder and red for disorder. As inputs for the modeling, the sequences [ABQ55991](#), [ABQ54733](#), and [ABQ54423](#) from the NCBI Database were used for Lpc2061, FlaA, and SspB, respectively. As the interactions

occur in membrane fractions, we scanned the sequences for cleavage sites using SignalP 6.0 (29). For Lpc2061, we identified a cleavage site at residue 24. Accordingly, the sequence starting from residue 25 of ABQ55991 was used for the modeling. Since no cleavage sites were found in FlaA or in SspB, the entire sequences were used as inputs. Protein visualizations were created using PyMol (32).

**Molecular docking.** To investigate the interactions of Lpc2061, SspB, and FlaA with Mip *in silico*, the global docking protocol from the Rosetta framework was used to generate an ensemble of 100k poses, each (33). This method fixes one protein and tries to randomly place the other mobile molecule on its surface so that the energy function is minimized. For visualization, the surface of Mip was colored per residue by the interface score of the best pose in which the docking partner had a contact with Mip. The docking scores were again normalized for visualization by the minimum and maximum values of the respective ensemble in the interval from best interface score (−1) to worst interface score (+1). The best interface score per residue over all of the poses was used for the surface coloring, which indicates good or bad contact sites with the interaction partners. The protein visualizations were created with PyMol (32).

**Molecular dynamics simulations.** Molecular dynamics (MD) simulations of the refined best pose from the global docking ensemble were performed in GROMACS (69) by using the CHARMM36 force field (70). After placing the molecule inside a dodecahedron with periodic boundary conditions, ions were added to neutralize the overall charge. After equilibration for 100 ps in the NVT [(number of particles) × (volume) × (temperature)] and then the NPT [(number of particles) × (pressure) × (temperature)] ensembles, the production run was performed for 500 ns at 303 K and 1 bar. To analyze the stability of the MD simulation, the root mean square deviation (RMSD), measuring the average deviation of each atom from a reference, was used (71). To analyze the quality of the protein-protein complexes, the interface RMSD (i-RMSD) was used. Furthermore, the quality of a protein-protein docking result was judged by its interface RMSD (i-RMSD). This was fitting for evaluating the docking poses (72), as the i-RMSD was successfully used to differentiate between native and nonnative structures. The i-RMSD is defined as the RMSD of only the atoms within the protein-protein interface (i.e., having an atom from the according touching protein in a 10 Å vicinity). As a third piece of quantitative information, we also visualized the counts of such contacts over the simulation time. These three quantities were evaluated for all MD simulations using custom-written Python scripts based on the Biotite package (73). The protein visualizations were created using PyMol (32).

**Statistical analysis.** The calculated concentrations of the isolated flagella were compared statistically. The repetitive measurements were statistically analyzed using a one-way analysis of variance (ANOVA) with Dunnett's multiple-comparison test by randomized blocks in GraphPad version 8.2.0 for Windows. The comparisons are based on a statistical significance cutoff of  $P \leq 0.05$ .

## SUPPLEMENTAL MATERIAL

Supplemental material is available online only.

**SUPPLEMENTAL FILE 1**, MP4 file, 12.6 MB.

**SUPPLEMENTAL FILE 2**, MP4 file, 7.8 MB.

**SUPPLEMENTAL FILE 3**, MP4 file, 12.4 MB.

**SUPPLEMENTAL FILE 4**, MP4 file, 4.5 MB.

**SUPPLEMENTAL FILE 5**, MP4 file, 5.1 MB.

**SUPPLEMENTAL FILE 6**, MP4 file, 7 MB.

**SUPPLEMENTAL FILE 7**, MP4 file, 7 MB.

**SUPPLEMENTAL FILE 8**, MP4 file, 8.7 MB.

**SUPPLEMENTAL FILE 9**, MP4 file, 13.4 MB.

**SUPPLEMENTAL FILE 10**, PDF file, 1.7 MB.

## ACKNOWLEDGMENTS

This research was funded by “Rahmenprogramm Gesundheitsforschung” of the Bundesministerium für Bildung und Forschung (BMBF), grant number 16GW0213. Computations were conducted on the Lichtenberg high performance computer of the TU Darmstadt, Germany.

## REFERENCES

- Mondino S, Schmidt S, Rolando M, Escoll P, Gomez-Valero L, Buchrieser C. 2020. Legionnaires' disease: state of the art knowledge of pathogenesis mechanisms of *Legionella*. *Annu Rev Pathol* 15:439–466. <https://doi.org/10.1146/annurev-pathmechdis-012419-032742>.
- Taylor M, Ross K, Bentham R. 2009. *Legionella*, protozoa, and biofilms: interactions within complex microbial systems. *Microb Ecol* 58:538–547. <https://doi.org/10.1007/s00248-009-9514-z>.
- Hilbi H, Hoffmann C, Harrison CF. 2011. *Legionella* spp. outdoors: colonization, communication and persistence. *Environ Microbiol Rep* 3:286–296. <https://doi.org/10.1111/j.1758-2229.2011.00247.x>.
- Phin N, Parry-Ford F, Harrison T, Stagg HR, Zhang N, Kumar K, Lortholary O, Zumla A, Abubakar I. 2014. Epidemiology and clinical management of Legionnaires' disease. *Lancet Infect Dis* 14:1011–1021. [https://doi.org/10.1016/S1473-3099\(14\)70713-3](https://doi.org/10.1016/S1473-3099(14)70713-3).
- Pagnier I, Merchat M, La Scola B. 2009. Potentially pathogenic amoeba-associated microorganisms in cooling towers and their control. *Future Microbiol* 4:615–629. <https://doi.org/10.2217/fmb.09.25>.
- Aurass P, Gerlach T, Becher D, Voigt B, Karste S, Bernhardt J, Riedel K, Hecker M, Flieger A. 2016. Life stage-specific proteomes of *Legionella pneumophila* reveal a highly differential abundance of virulence-associated Dot/

- Icm effectors. *Mol Cell Proteomics* 15:177–200. <https://doi.org/10.1074/mcp.M115.053579>.
7. Swart AL, Harrison CF, Eichinger L, Steinert M, Hilb H. 2018. *Acanthamoeba* and *Dictyostelium* as cellular models for *Legionella* infection. *Front Cell Infect Microbiol* 8:61. <https://doi.org/10.3389/fcimb.2018.00061>.
  8. Swanson MS, Hammer BK. 2000. *Legionella pneumophila* pathogenesis: a fateful journey from amoebae to macrophages. *Annu Rev Microbiol* 54:567–613. <https://doi.org/10.1146/annurev.micro.54.1.567>.
  9. Jäger J, Marwitz S, Tiefenau J, Rasch J, Shevchuk O, Kugler C, Goldmann T, Steinert M. 2014. Human lung tissue explants reveal novel interactions during *Legionella pneumophila* infections. *Infect Immun* 82:275–285. <https://doi.org/10.1128/IAI.00703-13>.
  10. Hoppe J, Ünal CM, Thiem S, Grimpe L, Goldmann T, Gaßler N, Richter M, Shevchuk O, Steinert M. 2017. PliY1 promotes *Legionella pneumophila* infection of human lung tissue explants and contributes to bacterial adhesion, host cell invasion, and twitching motility. *Front Cell Infect Microbiol* 7:63. <https://doi.org/10.3389/fcimb.2017.00063>.
  11. Scheithauer L, Thiem S, Schmelz S, Dellmann A, Büsow K, Brouwer RMHJ, Ünal CM, Blankenfeldt W, Steinert M. 2021. Zinc metalloprotease ProA of *Legionella pneumophila* increases alveolar septal thickness in human lung tissue explants by collagen IV degradation. *Cell Microbiol* 23:e13313. <https://doi.org/10.1111/cmi.13313>.
  12. Cianciotto NP, Eisenstein BI, Mody CH, Toews GB, Engleberg NC. 1989. A *Legionella pneumophila* gene encoding a species-specific surface protein potentiates initiation of intracellular infection. *Infect Immun* 57:1255–1262. <https://doi.org/10.1128/iai.57.4.1255-1262.1989>.
  13. Engleberg NC, Carter C, Weber DR, Cianciotto NP, Eisenstein BJ. 1989. DNA sequence of *mip*, a *Legionella pneumophila* gene associated with macrophage infectivity. *Infect Immun* 57:1263–1270. <https://doi.org/10.1128/iai.57.4.1263-1270.1989>.
  14. Cianciotto NP, Fields BS. 1992. *Legionella pneumophila mip* gene potentiates intracellular infection of protozoa and human macrophages. *Proc Natl Acad Sci U S A* 89:5188–5191. <https://doi.org/10.1073/pnas.89.11.5188>.
  15. Fischer G, Bang H, Ludwig B, Mann K, Hacker J. 1992. Mip protein of *Legionella pneumophila* exhibits peptidyl-prolyl-*cis/trans* isomerase (PPIase) activity. *Mol Microbiol* 6:1375–1383. <https://doi.org/10.1111/j.1365-2958.1992.tb00858.x>.
  16. Wintermeyer E, Ludwig B, Steinert M, Schmidt B, Fischer G, Hacker J. 1995. Influence of site specifically altered Mip proteins on intracellular survival of *Legionella pneumophila* in eukaryotic cells. *Infect Immun* 63:4576–4583. <https://doi.org/10.1128/iai.63.12.4576-4583.1995>.
  17. Riboldi-Tunnicliffe A, König B, Jessen S, Weiss MS, Rahfeld J, Hacker J, Fischer G, Hilgenfeld R. 2001. Crystal structure of Mip, a prolylisomerase from *Legionella pneumophila*. *Nat Struct Biol* 8:779–783. <https://doi.org/10.1038/nsb0901-779>.
  18. Helbig JH, Lück PC, Steinert M, Jacobs E, Witt M. 2001. Immunolocalization of the Mip protein of intracellularly and extracellularly grown *Legionella pneumophila*. *Lett Appl Microbiol* 32:83–88. <https://doi.org/10.1046/j.1472-765x.2001.00861.x>.
  19. Köhler R, Fanghänel J, König B, Lüneberg E, Frosch M, Rahfeld J-U, Hilgenfeld R, Fischer G, Hacker J, Steinert M. 2003. Biochemical and functional analyses of the Mip protein: influence of the N-terminal half and of peptidylprolyl isomerase activity on the virulence of *Legionella pneumophila*. *Infect Immun* 71:4389–4397. <https://doi.org/10.1128/IAI.71.8.4389-4397.2003>.
  20. Galka F, Wai SN, Kusch H, Engelmann S, Hecker M, Schmeck B, Hippenstiel S, Uhlin BE, Steinert M. 2008. Proteomic characterization of the whole secretome of *Legionella pneumophila* and functional analysis of outer membrane vesicles. *Infect Immun* 76:1825–1836. <https://doi.org/10.1128/IAI.01396-07>.
  21. Schmidt B, Tradler T, Rahfeld JU, Ludwig B, Jain B, Mann K, Rücknagel KP, Janowski B, Schierhorn A, Küllertz G, Hacker J, Fischer G. 1996. A cyclophilin-like peptidyl-prolyl *cis/trans* isomerase from *Legionella pneumophila*: characterization, molecular cloning and overexpression. *Mol Microbiol* 21:1147–1160. <https://doi.org/10.1046/j.1365-2958.1996.00061.x>.
  22. Fischer G, Tradler T, Zarnt T. 1998. The mode of action of peptidyl prolyl *cis/trans* isomerases in vivo: binding vs. catalysis. *FEBS Lett* 426:17–20. [https://doi.org/10.1016/s0014-5793\(98\)00242-7](https://doi.org/10.1016/s0014-5793(98)00242-7).
  23. Schiene-Fischer C, Aumüller T, Fischer G. 2013. Peptide bond *cis/trans* isomerases: a biocatalysis perspective of conformational dynamics in proteins. *Top Curr Chem* 328:35–67. [https://doi.org/10.1007/128\\_2011\\_151](https://doi.org/10.1007/128_2011_151).
  24. Ceymann A, Horstmann M, Ehes P, Schweimer K, Paschke A-K, Steinert M, Faber C. 2008. Solution structure of the *Legionella pneumophila* Mip-rapamycin complex. *BMC Struct Biol* 8:17. <https://doi.org/10.1186/1472-6807-8-17>.
  25. Horstmann M, Ehes P, Schweimer K, Steinert M, Kamphausen T, Fischer G, Hacker J, Rösch P, Faber C. 2006. Domain motions of the Mip protein from *Legionella pneumophila*. *Biochemistry* 45:12303–12311. <https://doi.org/10.1021/bi060818i>.
  26. Wagner C, Khan AS, Kamphausen T, Schmausser B, Unal C, Lorenz U, Fischer G, Hacker J, Steinert M. 2007. Collagen binding protein Mip enables *Legionella pneumophila* to transmigrate through a barrier of NCI-H292 lung epithelial cells and extracellular matrix. *Cell Microbiol* 9:450–462. <https://doi.org/10.1111/j.1462-5822.2006.00802.x>.
  27. Söderberg MA, Cianciotto NP. 2008. A *Legionella pneumophila* peptidyl-prolyl *cis-trans* isomerase present in culture supernatants is necessary for optimal growth at low temperatures. *Appl Environ Microbiol* 74:1634–1638. <https://doi.org/10.1128/AEM.02512-07>.
  28. Ünal C, Schwedhelm KF, Thiele A, Weiwad M, Schweimer K, Frese F, Fischer G, Hacker J, Faber C, Steinert M. 2011. Collagen IV-derived peptide binds hydrophobic cavity of *Legionella pneumophila* Mip and interferes with bacterial epithelial transmigration. *Cell Microbiol* 13:1558–1572. <https://doi.org/10.1111/j.1462-5822.2011.01641.x>.
  29. Teufel F, Almagro Armenteros JJ, Johansen AR, Gislason MH, Pihl SI, Tsirigos KD, Winther O, Brunak S, von Heijne G, Nielsen H. 2022. SignalP 6.0 predicts all five types of signal peptides using protein language models. *Nat Biotechnol* 40:1023–1025. <https://doi.org/10.1038/s41587-021-01156-3>.
  30. Appelt S, Heuner K. 2017. The flagellar regulon of *Legionella* - a review. *Front Cell Infect Microbiol* 7:454. <https://doi.org/10.3389/fcimb.2017.00454>.
  31. Bolon DN, Grant RA, Baker TA, Sauer RT. 2004. Nucleotide-dependent substrate handoff from the SspB adaptor to the AAA+ ClpXP protease. *Mol Cell* 16:343–350. <https://doi.org/10.1016/j.molcel.2004.10.001>.
  32. Schrödinger L, DeLano W. 2020. The PyMol Molecular Graphics System, Version 2.0 Schrödinger LLC, available at: <http://www.pymol.org/pymol>.
  33. Leaver-Fay A, Tyka M, Lewis SM, Lange OF, Thompson J, Jacak R, Kaufman K, Renfrew PD, Smith CA, Sheffler W, Davis IW, Cooper S, Treuille A, Mandell DJ, Richter F, Ban Y-EA, Fleishman SJ, Corn JE, Kim DE, Lyskov S, Berrondo M, Mentzer S, Popović Z, Havranek JJ, Karanicas J, Das R, Meiler J, Kortemme T, Gray JJ, Kuhlman B, Baker D, Bradley P. 2011. Rosetta3: an object-oriented software suite for the simulation and design of macromolecules. *Methods Enzymol* 487:545–574. <https://doi.org/10.1016/B978-0-12-381270-4.00019-6>.
  34. Wang F, Burrage AM, Postel S, Clark RE, Orlova A, Sundberg EJ, Kearns DB, Egelman EH. 2017. A structural model of flagellar filament switching across multiple bacterial species. *Nat Commun* 8:960. <https://doi.org/10.1038/s41467-017-01075-5>.
  35. Dietrich C, Heuner K, Brand B, Hacker J, Steinert M. 2001. Flagellum of *Legionella pneumophila* positively affects the early phase of infection of eukaryotic host cells. *Infect Immun* 69:2116–2122. <https://doi.org/10.1128/IAI.69.4.2116-2122.2001>.
  36. Cahoon LA, Freitag NE. 2015. Identification of conserved and species-specific functions of the *Listeria monocytogenes* PrsA2 secretion chaperone. *Infect Immun* 83:4028–4041. <https://doi.org/10.1128/IAI.00504-15>.
  37. Wiemels RE, Cech SM, Meyer NM, Burke CA, Weiss A, Parks AR, Shaw LN, Carroll RK. 2017. An intracellular peptidyl-prolyl *cis/trans* isomerase is required for folding and activity of the *Staphylococcus aureus* secreted virulence factor nuclease. *J Bacteriol* 199:e00453-16. <https://doi.org/10.1128/JB.00453-16>.
  38. Stewart DE, Sarkar A, Wampler JE. 1990. Occurrence and role of *cis* peptide bonds in protein structures. *J Mol Biol* 214:253–260. [https://doi.org/10.1016/0022-2836\(90\)90159-J](https://doi.org/10.1016/0022-2836(90)90159-J).
  39. Ünal CM, Steinert M. 2014. Microbial peptidyl-prolyl *cis/trans* isomerases (PPIases): virulence factors and potential alternative drug targets. *Microbiol Mol Biol Rev* 78:544–571. <https://doi.org/10.1128/MMBR.00015-14>.
  40. Ünal CM, Karagöz MS, Berge M, Priebe C, Borrero De Acuna JM, Wissing J, Jänsch L, Jahn D, Steinert M. 2019. Pleiotropic *Clostridioides difficile* cyclophilin PpiB controls cysteine-tolerance, toxin production, the central metabolism and multiple stress responses. *Front Pharmacol* 10:340. <https://doi.org/10.3389/fphar.2019.00340>.
  41. Bzdyl NM, Scott NE, Norville IH, Scott AE, Atkins T, Pang S, Sarovich DS, Coombs G, Inglis TJJ, Kahler CM, Sarkar-Tyson M. 2019. Peptidyl-prolyl isomerase *ppiB* is essential for proteome homeostasis and virulence in *Burkholderia pseudomallei*. *Infect Immun* 87:e00528-19. <https://doi.org/10.1128/IAI.00528-19>.

42. Únal CM, Berges M, Smit N, Schiene-Fischer C, Priebe C, Strowig T, Jahn D, Steinert M. 2018. PrsA2 (CD630\_35000) of *Clostridioides difficile* is an active parvulin-type PPIase and a virulence modulator. *Front Microbiol* 9: 2913. <https://doi.org/10.3389/fmicb.2018.02913>.
43. Debroy S, Aragon V, Kurtz S, Cianciotto NP. 2006. *Legionella pneumophila* Mip, a surface-exposed peptidylproline cis-trans-isomerase, promotes the presence of phospholipase C-like activity in culture supernatants. *Infect Immun* 74:5152–5160. <https://doi.org/10.1128/IAI.00484-06>.
44. Rasch J, Únal CM, Klages A, Karśli Ü, Heinsohn N, Brouwer RMHJ, Richter M, Dellmann A, Steinert M. 2019. PPIases Mip and PpiB of *Legionella pneumophila* contribute to surface translocation, growth at suboptimal temperature and infection. *Infect Immun* 15 pii:IAI 00939-17.
45. Rasch J, Krüger S, Fontvieille D, Únal CM, Michel R, Labrosse A, Steinert M. 2016. *Legionella*-protozoa-nematode interactions in aquatic biofilms and influence of Mip on *Caenorhabditis elegans* colonization. *Int J Med Microbiol* 306:443–451. <https://doi.org/10.1016/j.ijmm.2016.05.012>.
46. Scheuplein NJ, Bzdyl NM, Kibble EA, Lohr T, Holzgrabe U, Sarkar-Tyson M. 2020. Targeting protein folding: a novel approach for the treatment of pathogenic bacteria. *J Med Chem* 63:13355–13388. <https://doi.org/10.1021/acs.jmedchem.0c00911>.
47. Rasch J, Theuerkorn M, Únal C, Heinsohn N, Tran S, Fischer G, Weiwad M, Steinert M. 2015. Novel cycloheximide derivatives targeting the moonlighting protein Mip exhibit specific antimicrobial activity against *Legionella pneumophila*. *Front Bioeng Biotechnol* 3(41). <https://doi.org/10.3389/fbioe.2015.00041>.
48. Rasch J, Únal C, Steinert M. 2014. Peptidylprolyl cis-trans isomerases of *Legionella pneumophila*: virulence, moonlighting and novel therapeutic targets. *Biochem Soc Trans* 42:1728–1733. <https://doi.org/10.1042/BST20140202>.
49. Juli C, Sippel M, Jäger J, Thiele A, Weiwad M, Schweimer K, Rösch P, Steinert M, Sotriffer CA, Holzgrabe U. 2011. Pipecolic acid derivatives as small-molecule inhibitors of the *Legionella* MIP protein. *J Med Chem* 54: 277–283. <https://doi.org/10.1021/jm101156y>.
50. Pomplun S, Sippel C, Hähle A, Tay D, Shima K, Klages A, Únal CM, Rieß B, Toh HT, Hansen G, Yoon HS, Bracher A, Preiser PR, Rupp J, Steinert M, Hausch F. 2018. Chemogenomic profiling of human and microbial FK506-binding proteins. *J Med Chem* 61:3660–3673. <https://doi.org/10.1021/acs.jmedchem.8b00137>.
51. Levchenko I, Seidel M, Sauer RT, Baker TA. 2000. A specificity-enhancing factor for the ClpXP degradation machine. *Science* 289:2354–2356. <https://doi.org/10.1126/science.289.5488.2354>.
52. Yin J, Ding M, Zha F, Zhang J, Meng Q, Yu Z. 2021. Stringent starvation protein regulates prodiginine biosynthesis via affecting siderophore production in *Pseudoalteromonas* sp. strain R3. *Appl Environ Microbiol* 87: e02949-20. <https://doi.org/10.1128/AEM.02949-20>.
53. Scherer CA, Cooper E, Miller SI. 2000. The *Salmonella* type III secretion translocator protein SspC is inserted into the epithelial cell plasma membrane upon infection. *Mol Microbiol* 37:1133–1145. <https://doi.org/10.1046/j.1365-2958.2000.02066.x>.
54. Tomoyasu T, Ohkishi T, Ukyo Y, Tokumitsu A, Takaya A, Suzuki M, Sekiya K, Matsui H, Kutsukake K, Yamamoto T. 2002. The ClpXP ATP-dependent protease regulates flagellum synthesis in *Salmonella enterica* serovar Typhimurium. *J Bacteriol* 184:645–653. <https://doi.org/10.1128/JB.184.3.645-653.2002>.
55. Molofsky AB, Shetron-Rama LM, Swanson MS. 2005. Components of the *Legionella pneumophila* flagellar regulon contribute to multiple virulence traits, including lysosome avoidance and macrophage death. *Infect Immun* 73:5720–5734. <https://doi.org/10.1128/IAI.73.9.5720-5734.2005>.
56. Hammer BK, Tateda ES, Swanson MS. 2002. A two-component regulator induces the transmission phenotype of stationary-phase *Legionella pneumophila*. *Mol Microbiol* 44:107–118. <https://doi.org/10.1046/j.1365-2958.2002.02884.x>.
57. Heuner K, Steinert M. 2003. The flagellum of *Legionella pneumophila* and its link to the expression of the virulent phenotype. *Int J Med Microbiol* 293:133–143. <https://doi.org/10.1078/1438-4221-00259>.
58. Forstneric V, Ivčak-Kocjan K, Plaper T, Jerala R, Bencina M. 2017. The role of the C-terminal D0 domain of flagellin in activation of Toll like receptor 5. *PLoS Pathog* 13:e1006574. <https://doi.org/10.1371/journal.ppat.1006574>.
59. Song WS, Jeon JY, Namgung B, Hong M, Yoon S. 2017. A conserved TLR5 binding and activation hot spot on flagellin. *Scient Rep* 7:40878.
60. Borrero-de Acuña JM, Rohde M, Wissing J, Jänsch L, Schobert M, Molinari G, Timmis KN, Jahn M, Jahn D. 2016. Protein network of the *Pseudomonas aeruginosa* denitrification apparatus. *J Bacteriol* 198:1401–1413. <https://doi.org/10.1128/JB.00055-16>.
61. Hanahan D. 1983. Studies on transformation of *Escherichia coli* with plasmids. *J Mol Biol* 166:557–580. [https://doi.org/10.1016/s0022-2836\(83\)80284-8](https://doi.org/10.1016/s0022-2836(83)80284-8).
62. Montie TC, Craven RC, Holder IA. 1982. Flagellar preparations from *Pseudomonas aeruginosa*: isolation and characterization. *Infect Immun* 35:281–288. <https://doi.org/10.1128/iai.35.1.281-288.1982>.
63. Helbig JH, Ludwig B, Lück PC, Groh A, Witzleb W, Hacker J. 1995. Monoclonal antibodies to *Legionella* Mip proteins recognize genus- and species-specific epitopes. *Clin Diagn Lab Immunol* 2:160–165. <https://doi.org/10.1128/cdli.2.2.160-165.1995>.
64. Neuhoff V, Arold N, Taube D, Ehrhardt W. 1988. Improved staining of proteins in polyacrylamide gels including isoelectric focusing gels with clear background at nanogram sensitivity using Coomassie Brilliant Blue G-250 and R-250. *Electrophoresis* 9:255–262. <https://doi.org/10.1002/elps.1150090603>.
65. Blum H, Beier H, Gross HJ. 1987. Improved silver staining of plant proteins RNA and ist in polyacrylamide gels. *Electrophoresis* 8:93–99. <https://doi.org/10.1002/elps.1150080203>.
66. Cianciotto NP, Bangsberg JM, Eisenstein BI, Engleberg NC. 1990. Identification of mip-like genes in the genus *Legionella*. *Infect Immun* 58:2912–2918. <https://doi.org/10.1128/iai.58.9.2912-2918.1990>.
67. Heuner K, Bender-Beck L, Brand BC, Lück PC, Mann KH, Marre R, Ott M, Hacker J. 1995. Cloning and genetic characterization of the flagellum subunit gene (flaA) of *Legionella pneumophila* serogroup 1. *Infect Immun* 63: 2499–2507. <https://doi.org/10.1128/iai.63.7.2499-2507.1995>.
68. Jumper J, Evans R, Pritzel A, Green T, Figurnov M, Ronneberger O, Tunyasuvunakool K, Bates R, Židek A, Potapenko A, Bridgland A, Meyer C, Kohl SAA, Ballard AJ, Cowie A, Romera-Paredes B, Nikolov S, Jain R, Adler J, Back T, Petersen S, Reiman D, Clancy E, Zielinski M, Steinegger M, Pacholska M, Berghammer T, Bodenstein S, Silver D, Vinyals O, Senior AW, Kavukcuoglu K, Kohli P, Hassabis D. 2021. Highly accurate protein structure prediction with AlphaFold. *Nature* 596:583–589. <https://doi.org/10.1038/s41586-021-03819-2>.
69. Abraham MJ, Murtola T, Schulz R, Páll S, Smith JC, Hess B, Lindahl E. 2015. GROMACS: high performance molecular simulations through multi-level parallelism from laptops to supercomputers. *SoftwareX* 1–2:19–25. <https://doi.org/10.1016/j.softx.2015.06.001>.
70. Vanommeslaeghe K, Hatcher E, Acharya C, Kundu S, Zhong S, Shim J, Darian E, Guvench O, Lopes P, Vorobyov I, Mackerell AD. 2010. CHARMM general force field: a force field for drug-like molecules compatible with the CHARMM all-atom additive biological force fields. *J Comput Chem* 31: 671–690. <https://doi.org/10.1002/jcc.21367>.
71. Benson NC, Daggett VA. 2012. Comparison of multiscale methods for the analysis of molecular dynamics simulations. *J Phys Chem B* 116:8722–8731. <https://doi.org/10.1021/jp302103t>.
72. Jandova Z, Vargiu AV, Bonvin AMJJ. 2021. Native or non-native protein-protein docking models? Molecular dynamics to the rescue. *J Chem Theory Comput* 17:5944–5954. <https://doi.org/10.1021/acs.jctc.1c00336>.
73. Kunzmann P, Hamacher K. 2018. Biotite: a unifying open source computational biology framework in Python. *BMC Bioinformatics* 19:346. <https://doi.org/10.1186/s12859-018-2367-z>.
74. Jepras RI, Fitzgeorge RB, Baskerville A. 1985. A comparison of virulence of two strains of *Legionella pneumophila* based on experimental aerosol infection of guinea-pigs. *J Hyg (Lond)* 95:29–38. <https://doi.org/10.1017/s002217240062252>.